Interactive comment on "The Influence of Simulated Surface Dust Lofting Erodible Fraction on Radiative Forcing" by Stephen M. Saleeby et al.

Reviewer comments below are in standard black font, while the author responses are in blue italic font for contrast.

General reply to reviewers based on overarching comments:

We thank the reviewers for their time in examining our manuscript and offering constructive criticism, comments, and suggestions. We feel that reviewer comments have led to an improved manuscript. As will be discussed in detail below in response to specific comments and questions, this paper presents a theoretical modeling study placed in the context of a dust lofting event over the Arabian Peninsula that explores the potential radiative response to variable dust loading using dust lofting models and dust-sensitive radiation schemes embedded within sophisticated high-resolution model environments. The main goal of the paper is to examine the mean differences in radiative quantities and atmospheric temperature resulting from differences in dust loading that result from applying different dust erodible fraction datasets to the lofting model.

While the Arabian Peninsula is well-known for its expansive dust storms, few dust lofting studies have been performed over this region. This is, perhaps, because aerosol related data in this region are limited. As such, we have provided a more qualitative model comparison to the limited aerosol observations in the area in order to broadly demonstrate that one of the models (RAMS) does a favorable job in simulating dust lofting when the dust erodible fraction is constrained by geographical datasets, while noting that precisely simulating the magnitude and location of individual dust plumes is incredibly difficult. Following this, the RAMS model was then used to investigate dust radiative effects in the simulated environment. It is not our intent to determine which dataset leads to the best model representation of dust lofting. Walker et al. (2009) provide such an assessment with regards to dust lofting and surface visibility. Our focus is on determining the potential range of dust radiative effects by comparing a simulation with no-dust to those with varying amounts of dust generated by use of different specifications of surface dust erodible fraction.

Overall, we have worked to more clearly frame the focus of this paper as a theoretical examination of dust radiative effects in a case study context, while noting that dust AOD observations are limited, yet they compare favorably to RAMS simulations when dust erodible fraction appropriately constrains the amount of lofting.

Anonymous Referee #1

Received and published: 5 February 2019

The authors present results of a regional NWP model simulations over the Arabian Peninsula region, including mineral dust aerosol, for a case study during August 2015. They test sensitivity of dust simulations to two different models used, and to three different dust source representations. They compare these results to observations. One of the models is then used to examine the radiative effects of the dust in a cloud-free region, with a particular emphasis on radiative divergence, net radiative flux, and vertical temperature profiles, contrasting the differences due to the different dust source representations.

The paper is mostly clearly and succinctly written, and easy to follow in terms of methodology and analysis. The interpretation of impacts of dust loading on radiative fluxes, vertical temperature profile, and surface fluxes are a valuable addition to the literature and will help inform future studies on the potential impact of dust on cloud development. However, the earlier part of the paper (the impact of dust source representation on dust loading and AOD) is less clearly analyzed and the main conclusions of this section are a little weak. The justification for including the "idealized" lofting method is unclear (see major points below). The observations are not really sufficient to inform which of the two realistic lofting experiments (Ginoux and Walker) performs better and as such the first part of the paper is not particularly illuminating.

We thank this reviewer for your overall assessment of this manuscript. Our general reply to reviewers at the top of this document is meant to provide focus on the intent of the paper while addressing the concerns regarding the comparisons to limited observations. We have revised the manuscript to help focus the direction and intent of the paper and address the utility of the Idealized lofting experiment, as noted above.

The abstract is fairly poor in describing the experiments the authors have conducted, why these were done, and their conclusions. A number of minor clarifications are necessary and are detailed below. However, with some additional clarifications and explanations the authors should be able to suitably address all these points and provide a paper suitable for ACP.

We have examined the abstract and have rewritten it to better describe the motivation, experiments, and conclusions. We have also responded to each specific comment below.

Major points

1) Idealized lofting

It is not clear why the authors choose to implement the 'idealized' lofting method when it generates such unrealistic results, and is also physically unrealistic. I suspect it is because this 'extreme' case becomes useful in section 4 when evaluating the radiative fluxes in terms of understanding how the system reacts to a 'kick'. Much more justification and explanation of the idealized method should be provided, as well as a statement that the authors do not expect it to respond realistically, and that it is retained for evaluation of 'extreme' purposes in section 4 (if that is the case). In terms of conclusions and abstract, it is not surprising that the idealized case produces inferior results – this is not a scientific finding.

We noted in the discussion of the simulations that the "Idealized" lofting method was included as one of our experiments since this method has been used in another study that simulates idealized conditions (e.g. Seigel and van den Heever 2012). In idealized simulations the "Idealized" lofting method, that can loft dust in any grid cell containing dry soil, certain clay fractions, and low vegetation, has been shown to produce reasonable amounts of dust for localized dust events. It seems fair to extend this to a case study for testing to examine the upper *end of potential dust lofting, even if this may be unrealistic. As such, we have revised the manuscript to present this as being an upper limit to dust lofting that could occur in this model setting, and then examine the upper limit of radiative response. We have modified the text to better clarify this motivation.*

2) Abstract

The abstract needs a complete re-write to follow a typical structure of description of a) the field/problem, b) description of experiments carried out and why, and c) results found and their significance. Currently a) and b) are completely missing. Idealized lofting, if mentioned in the abstract, should be explained. It would be useful to relate 'extreme' and 'moderate' dust references to specific AOD ranges. L23-25 – this statement is not justified. The authors have not shown that the higher resolution source database produced better results (though the word 'detail' is ambiguous) – simply that it provided more spatial variability in the dust load. The fact that the Ginoux and Walker uplift experiments do not produce particularly difference radiative effects should be stated (and also discussed in the paper).

The abstract has been re-written to provide a concise summary of the work presented in this manuscript. Also, we have added discussion regarding the similarities in the results comparing the Ginoux and Walker experiments.

3) Significance of Section 3

Overall the observational evidence for evaluating the Ginoux vs. Walker uplift experiments is fairly weak. The Walker simulation provides much greater spatial variability due to the higher resolution of the input surface data compared to the Ginoux dataset. However, the sparsity of the data over the region prevents the authors from reliably evaluating whether one dataset is better than the other. The MODIS data shown is rather patchy and also only show for part of the simulation region. The AERONET data is not conclusive in the evaluation and a small offset in model analysis region for the AERONET comparison produces significantly different results. The authors should either attempt to expand their observational comparison to inform the model comparison, or if this is not possible, modify the text and conclusions appropriately to say that lack of observations prevent a proper evaluation of the two dust source datasets. Even without being able to say which dataset is better, it is a useful finding that more resolution in surface dust source area translates to more spatial variability in the atmosphere, even after several days of transport.

Thank you for this comment. We agree that it would be desirable to have a more extensive AERONET array and better MODIS coverage. However, we have presented what limited observations are available for comparing dust. We have modified the text to highlight that observations are limited and thus our observational comparison is intended to be qualitative in nature. The single southern AERONET site provides us with only a single point comparison near the UAE / Persian Gulf dust plume. Performing grid point comparisons between models and observations often provides limited utility in events where key features, such as dust plumes, are slightly displaced in the simulations. In our case the simulated dust plume over the UAE and Persian Gulf is slightly displaced, but magnitudes of AOD are similar to the in-plume MODIS AODs. We have added text that addresses the limited nature of the observations and their comparisons to model results.

4) Comparison against literature
There is rather little comparison against other literature in general – this would add to the significance of the article – both in the context of implementing different dust source maps, and in terms of the radiative effect (Section 4) results.

Throughout the manuscript we have added more comparison between the results of this study and past work including some comparisons with the following papers: Slingo et al. (2006), Shell et al. (2007), Lau and Kim (2007), Marsham et al. (2016), Hansell et al. (2010), Kosmopoulos et al. (2017).

Minor points and clarifications

Title – I encourage the authors to make this clearer – e.g. remove 'erodible fraction' and possibly include 'and atmospheric loading' before 'radiative forcing'

We have changed the title to remove "erodible fraction" and include "and atmospheric loading".

P2L9 – dust can cause atmospheric cooling in the LW also

We have added a statement here to the effect that LW emission in the dust layer adds a cooling tendency within the dust layer, but warming effect via LW emission adjacent to the dust layer (e.g. Slingo et al. 2006; Wang et al. 2013).

Section 2.2 – GOCART should be briefly described (e.g. size bins, uplift scheme) to give the equivalent information provided on the dust scheme in RAMS.

We have added some text to section 2.1 to indicate that RAMS' dust scheme is largely based on GOCART with some additional modifications related to soil type, vegetation, and dust lofting size bins. WRF-Chem uses GOCART dust lofting. The details of GOCART dust lofting can be found in Ginoux et al. (2001) as referenced.

Section 2.3 – p5 L27 onwards – Does this mean that the erodible fraction over the whole land-domain is 100%? Please clarify.

In the Idealized simulation, the erodible fraction over the whole land domain is 1.0 (100%). This was done for the Seigel and van den Heever (2012) limited area domain and produced quite favorable dust amounts over a limited time frame involving outflows from deep convection. We have added text to section 2.3 to clarify this. We have also placed the Idealized simulation in the context of representing the expected upper bound on dust lofting in this type of case study. We found it quite informative to know the potential upper limit of radiative effects that could be expected within the given modeling framework and parameterization.

Section 2.3 – p5 L27-35 – more background should be provided on each of the 3 surface lofting methodologies/datasets, since this is a key process and result within the paper. E.g. How were the datasets produced? What are they based on? Why are they different. Is the Ginoux dataset the topographic low source function?

We have added into this section several sentences that clarify the application of the Idealized lofting method, the Ginoux method based on topographic depressions, and the Walker method based on manual satellite identification of dust lofted areas. Each of these methods has an associated citation for which the referenced paper can provide the intricate details of the lofting methods/databases.

Figure 2a – why are there lines around some of the grid boxes? Is this an artefact? It seems unphysical.

The lines are just an artifact of the plotting tool and the discrete application of Ginoux 1-deg gridded dust sources to the model grid.

P7L3 – refs to Fig 4a – it's pretty difficult to see the dust over the desert. It would be helpful to refer the reader to AOD figure 7 here too (see also comment about domain shown in fig 7).

The dust over the desert is, indeed, difficult to discern in the visible imagery due to the similar colors of the dust and land area. We have updated the text to also point to the MODIS imagery in Figure 7 that shows some of the dust presence associated with the two plumes.

P7L8-9 – could this also be the higher resolution between the reanalysis and the model runs?

The differences in the magnitude of the 1000mb temperature field between the reanalysis and model data are probably more the result of the differences in the representation of topography and the land surface parameterizations between the models used here and the model portion of the reanalysis technique. The differences in the horizontal variability and spatial details between the models and reanalysis are likely due to resolution differences. We have added text in the manuscript to clarify these differences.

P7L11-19 – The inclusion of the NAAPS plot is confusing and unhelpful. The inclusion of data from NAAPS is sudden and unexplained. Comparing a model to another model is not helpful. I suggest removing the NAAPS figure and text completely. It does not add anything to the paper.

We have removed all discussion and figures related to NAAPS.

P7L31-32 – 'In both models, the Walker simulations captures more dust mass detail with respect to the lofting locations due to the precise, high resolution nature of the database.' – This should be reworded. The simulation may show more 'detail' – (spatial variability is probably a better word) but there are no constraints to show that this is correct. Due to the source database being higher resolution, one would expect the atmospheric dust loading to be more spatially variable. The does not show it is better or correct though.

We have restated this sentence to note that the high-resolution Walker dust source database leads to the generation of comparatively greater fine-scale spatial variability in lofted dust in *association with known dust source locations. We have also added a statement that while there is increased precision in lofted locations with the Walker database, that does not imply that the net amount of lofted dust is more accurate than that lofted via the Ginoux database. Walker et al. (2009) provide such an assessment.*

P7L30 onwards – WRF results are quite different to RAMS – the authors should discuss this and attempt to explain why.

Yes, WRF and RAMS dust amounts and AOD are quite different. We state at the end of Section 3.1 that these differences exist and that there is a separate study under way to perform an extensive model inter-comparison involving RAMS, WRF, and another model as well. This type of model inter-comparison is beyond the scope of this paper and will appear in a separate manuscript in the future. However, we have also added a statement to the end of Section 3.1 which says that both RAMS and WRF use the dust lofting techniques of the GOCART model (Ginoux et al. 2001) and the same erodible fraction databases; as such, we speculate that the prediction of the near-surface wind speed, the soil moisture, dust deposition rates, and dust binning may all be playing a role in contributing to the differences. A separate in-depth study will help shed light on this.

P8L1-2 – See above points about NAAPS – no need for NAAPS data here. Actual observations should be used to verify simulations, no another model! (And if there are no observations, a simple statement to this effect is sufficient).

We have removed NAAPS from the paper and have noted in the paper the limited aerosol observations available for comparison.

P8L5 – does this mean that RAMS does not include radiative feedbacks of dust, onto dynamics, etc.?

No. It means that we used an offline model to compute diagnostic AOD for comparison with MODIS and AERONET. The RAMS model does not provide AOD as a standard output diagnostic, thus we had to generate this offline. However, the aerosols are radiatively interactive, thus, impacting the radiation flux profiles and providing feedbacks to the dynamics and thermodynamics. We have added a statement and reference in this regards in the section that describes the RAMS aerosol model.

P8L8 – refractive index at which wavelength? Assuming this is 500-550nm, the imaginary part is relatively high (e.g. see Song et al. 2018, Balkanski et al. 2017). This will impact the radiative results in section 4 by causing increased absorption and atmospheric heating, and should be discussed. E.g. Strong et al. (2018) show that small changes in optical properties can have huge effects on circulation.

This index of refraction is referring to the 550nm mentioned above on line 5 for the offline analysis of AOD. Per this reviewer question, we have added additional text and citations in section 2.1 regarding the use of a dust complex index of refraction of 1.53+0.0015i for dust for *wavelengths up to ~2000nm wavelength for generating RAMS lookup tables of aerosol optical properties. Further, we note that AOD is not sensitive to the imaginary index of refraction.*

P8L9 – 'spheroid-like index of refraction' – clarify this – index of refraction does not have a shape.

The wording has been changed in the text to clarify the assignment of the dust index of refraction used for computing AOD from our offline model of aerosol extinction.

P8L8-10 – what refractive index in the LW is used?

The AOD analysis was only done at 550nm. However, we have added text to Section 2.1 to better describe the assignment of the indices of refraction for dust at various wavelengths. As noted in a response above we use in RAMS a complex index of refraction of 1.53+0.0015i for dust up to ~2000nm. We state that Stokowski (2005) provides a plot of refractive index as it varies with wavelength in the RAMS model.

P8L15-16 – what dust optical properties are used in WRF?

We have added a statement in the text indicating that the dust real index of refraction for computing AOD at 550nm in WRF is set at 1.53.

P9L1 – 'similar predicted synoptic situations' – this doesn't seem justified – the streamlines are quite different between RAMS and WRF – and dust uplift is extremely sensitive to small differences in wind pattern, speed and strength.

We have modified this section and section 2.4 to better state the similarities and differences between the synoptic fields shown in figure 3. The streamlines are shown so as to demonstrate that both models produced the northerly flow associated with the Saudi dust plume and the southerly to south-westerly flow associated with the UAE plume. We have added statements in the text that address the differences in AOD between RAMS and WRF and offer speculation that differences in wind speed and other conditions could explain the differences in dust lofting between the models. As noted earlier, this involves an on-going model inter-comparison study for a separate manuscript.

P9L3 – 'trends' – which ones? The authors have only discussed differences between idealized vs. Ginoux/Walker, not Ginoux vs. Walker, which are clearly not the same for WRF and RAMS.

We have reworded this paragraph to better summarize the overarching differences between simulations and models and between modeled and observed dust AOD.

P9L24-27 – and also impacts the Walker expt more because there is more spatial variability in the atmospheric dust load?

We have added discussion throughout the manuscript regarding the differences between simulated Ginoux and Walker dust plume concentration and AOD. We specifically discuss that *the widespread, small erodible fraction with Ginoux dust data tend to produce more broad dust plumes with lower maximum AOD. The Walker data tend to generate more focused plumes with higher maximum AOD and greater spatial variability. This certainly impacts the interpretation of the grid point comparisons to AERONET sites.*

P12L33 – 'small warming' – how much?

We have added the detail that the small warming is ~0.3-0.4C for the Ginoux and Walker simulations compared to No-Dust.

Section 4 – there is no comparison between Ginoux vs. Walker results here – why not?

While some comparisons are made between the Ginoux and Walker results, they are noted as being quite similar compared to the Idealized simulation. Many places throughout section 4 indicate monotonic changes in radiative fluxes with dust loading, and we have noted that the mean dust loading in the analysis region increases from the Ginoux to Walker to Idealized simulations (see figure 9a dust profiles). The discussion of monotonic changes implicitly compares all three dust-lofting simulations to the No-Dust simulation and to each other. However, in the revised manuscript we have included additional statements to compare the Ginoux and Walker simulations.

Section 4 – are the radiative results consistent with other work? E.g. Marcham et al. (2016)?

We noted in section 4.2 that the reductions in shortwave radiation for the Ginoux and Walker simulations are similar to those seen in Slingo et al. (2006) and Kosmopoulos et al. (2017) for similar AOD. We added more detail to this to note that both studies show surface shortwave reductions of approximately 200-250W/m2 for dust AOD on the order of 1.5-2.5.

We have added more comparisons to past work that is comparable to this study including comparisons to shortwave and longwave fluxes as well as estimated heating rates. (e.g. Marsham et al. 2016, Hansell et al. 2010).

Conclusion – more text should be added to cover the results of the source dataset experiments – e.g. the effects of Walker vs. Ginoux simulations, and the fact that the Walker simulations produced more patchy dust loadings than Ginoux.

We have updated the conclusions to offer a more comprehensive summary of the results and include more summary of the differences between the Ginoux and Walker simulations.

Figures – take care that the same country boundaries are shown on all maps. E.g. fig 3 – the WRF plots show different country boundaries to the other plots. H and I do not show boundaries. Check ACP guidelines for international borders.

We have worked to make the country boundaries similar among the RAMS and WRF plots.

Figures 5-6 – the authors should show the analysis region on figures a-c

We have added the analysis region box to figures 5&6 panels a-c.

Fig 7 – why is the same geographical domain as figs 5-6 not shown? A larger area would be more appropriate, especially since the radiative analysis region is not even covered in fig 7.

The model AOD (figure 6) is available over the full simulation domain, but the MODIS AOD (figure 7) does not cover the full model domain, but rather a limited swath. We had zoomed in over the plumes to be able to see some of the higher AOD pixels associated with the Persian Gulf plume. However, we have modified the figure to show the full domain, which does provide a better view of the Saudi dust plume.

References

Balkanski, Y., et al.: Reevaluation of Mineral aerosol radiative forcings suggests a better agreement with satellite and AERONET data, Atmos. Chem. Phys., 7, 81-95, https://doi.org/10.5194/acp-7-81-2007, 2007.

Marsham, J. H., et al.: The contrasting roles of water and dust in controlling daily variations in radiative heating of the summertime Saharan heat low, Atmos. Chem. Phys., 16, 3563-3575, https://doi.org/10.5194/acp-16-3563-2016, 2016.

Song, Q., et al.: Net radiative effects of dust in the tropical North Atlantic based on integrated satellite observations and in situ measurements, Atmos. Chem. Phys., 18, 11303-11322, https://doi.org/10.5194/acp-18-11303-2018, 2018.

Strong, J. D. O., Vecchi, G. A., Ginoux, P. (2018). The climatological effect of Saha- ran dust on global tropical cyclones in a fully coupled GCM. Journal of Geophysical Research: Atmospheres, 123. https://doi.org/10.1029/2017JD027808

Interactive comment on “The Influence of Simulated Surface Dust Lofting Erodible Fraction on Radiative Forcing” by Stephen M. Saleeby et al.

Reviewer comments below are in standard black font, while the author responses are in blue italic font for contrast.

General reply to reviewers based on overarching comments:

We thank the reviewers for their time in examining our manuscript and offering constructive criticism, comments, and suggestions. We feel that reviewer comments have led to an improved manuscript. As will be discussed in detail below in response to specific comments and questions, this paper presents a theoretical modeling study placed in the context of a dust lofting event over the Arabian Peninsula that explores the potential radiative response to variable dust loading using dust lofting models and dust-sensitive radiation schemes embedded within sophisticated high-resolution model environments. The main goal of the paper is to examine the mean differences in radiative quantities and atmospheric temperature resulting from differences in dust loading that result from applying different dust erodible fraction datasets to the lofting model.

While the Arabian Peninsula is well-known for its expansive dust storms, few dust lofting studies have been performed over this region. This is, perhaps, because aerosol related data in this region are limited. As such, we have provided a more qualitative model comparison to the limited aerosol observations in the area in order to broadly demonstrate that one of the models (RAMS) does a favorable job in simulating dust lofting when the dust erodible fraction is constrained by geographical datasets, while noting that precisely simulating the magnitude and location of individual dust plumes is incredibly difficult. Following this, the RAMS model was then used to investigate dust radiative effects in the simulated environment. It is not our intent to determine which dataset leads to the best model representation of dust lofting. Walker et al. (2009) provide such an assessment with regards to dust lofting and surface visibility. Our focus is on determining the potential range of dust radiative effects by comparing a simulation with no-dust to those with varying amounts of dust generated by use of different specifications of surface dust erodible fraction.

Overall, we have worked to more clearly frame the focus of this paper as a theoretical examination of dust radiative effects in a case study context, while noting that dust AOD observations are limited, yet they compare favorably to RAMS simulations when dust erodible fraction appropriately constrains the amount of lofting.

Anonymous Referee #2

Received and published: 11 February 2019

The manuscript analyses the numerical simulations of dust lofting using erodible dust fraction as input and its impact on radiation during daytime hours and nighttime hours. The dust erodible faction is taken from dataset from three methods, namely, the “idealized”, “Ginoux”, and “Walker”. The numerical simulations are done with WRF and RAMS over the Arabian

Peninsula. Overall, the manuscript is well written, logically presented, and is interesting to read. I recommend the publication of this manuscript after considering the following suggestions:

1. I could not find any quantitative validation exercise between MODIS and Model AOD. Please clarify. Can the MODIS AOD be extracted at some of the stations and compared with Model data? It has also ben inferred in previous studies that MODIS data overpredicted AOD for regions predominant with dust (see Remer et al. 2005). Please take this into account while validation of the model. (Remer LA, Kaufman YJ, Tanré D, Matto S, Chu DA, Martins JV, Li RR, Ichoku C, Levy RC, Kleidman RG, Eck TF, Vermote E, Holben BN (2005) The MODIS aerosol algorithm, products, and validation. J Atmos Sci 62:947–973. https://doi.org/10.1175/JAS3385.1)

As reviewer 1 has pointed out, we have limited aerosol observations for validation of this dust event. We have included the two MODIS aerosol retrievals during this event that had the best available domain coverage. In the discussion of the MODIS data we cited that the retrievals have an uncertainly of ~20% over land and 10-15% over water. We have added citation of Remer et al. (2005) and noted potential MODIS AOD overestimation in high dust loading environments.

While the MODIS AOD is useful for a qualitative comparison of the UAE and Saudi dust plumes, the data is quite patchy and covers only a portion of the domain. We have also noted that the modeled dust plumes in the RAMS simulations are slightly displaced compared to the corresponding high AOD plumes in the MODIS overpasses. These factors are prohibitive towards producing a meaningful quantitative comparison. However, visual qualitative comparisons reveal that the RAMS Ginoux and Walker simulations generate dust plumes in the region of the observed plumes. Further, the modeled plumes have AODs in the 1.5-2.5 range across the bulk of the plumes, which is very similar to the range of AOD seen in the MODIS data. While the MODIS data may have uncertainties up to 20% over land, the retrieved high AOD values are co-located with dense plumes seen in the visible imagery in Figure 4 and denote these plumes as being substantial dust events. As such, this event is worth examining in the model with respect to the potential variability in radiative effects due to different specification of dust erodible fraction.

In addition, we have interpolated the MODIS pixels to the location of the Mezaira AERONET site and added these point observations to the MODIS AOD figure. The interpolated MODIS AOD values from both overpasses are lower than the AERONET values, but are still indicative of a substantial dust event. As we note in the manuscript, the MODIS data is being interpolated to a point location in an area with a tight gradient in AOD and in the vicinity of missing pixels. As such, we suspect the interpolation tends to under-represent the high AOD at the indicated times compared to AERONET.

2. A large underestimation is seen between model and AERONET AOD. What could be the reason for this? It will be nice if the authors could provide a quantitative validation, including bias and normalized mean error. How much is the uncertainty in AERONET AOD for regions predominant with dust? I suggest strengthening this Section by providing information from any available literature study as well. One of such studies, I recently found is by Kokkalis et al.,

(2018). Long-Term Ground-Based Measurements of Aerosol Optical Depth over Kuwait City. Remote Sensing, 10, 1807; DOI:10.3390/rs1011180710.

The main point in providing the grid point comparisons of AOD is to generally demonstrate the presence of an intense dust plume in the area in both the observations and the model. As discussed in the paper, grid point comparisons, while potentially useful, can be deceptive when making comparisons in areas of tight gradients and areas where simulated features such as dust plumes are reasonably represented in the model but are slightly displaced compared to the observed location. Here, the underestimation in the model compared to AERONET is largely due to the fact that the model generates a dust plume over the UAE / Persian Gulf region that is slightly displaced to the east. Further, in the Walker simulation, there's a substantial gradient in dust AOD along the edges of the plume. As shown in the AERONET figure, a simulated in-plume grid point time series to the east of the Mezaira location does indeed reveal the passage of an intense dust plume. Such comparisons can be useful, but need to be cautiously interpreted. We have added some details from the Kokkalis et al. paper that help shed light on AODs that represent a mean background state for this region as well as dust storm AOD values.

3. Also, why "Ginoux"' is larger than the "Walker" (refer to Figure 7c)? Please include some discussion on this.

We note that figure 7c is a time series for a single grid point, so any spatial displacement between simulations can produce somewhat deceptive differences at single locations. The simulated UAE plume is displaced a bit to the east of the Mezaira location shown in the time series. As noted in the text, the Walker simulation lofts dust in more precise locations and then transports those with the wind. As such, the Walker dust plume is narrow and somewhat displaced from the Mezaira location. The Ginoux simulations have lower erodible fraction than the Walker dust locations, but the Ginoux sources cover a much larger area. As such, the Ginoux plume near Mezaira is more broadly dispersed but with a lower maximum AOD compared to the plume in the Walker simulation. We have added discussion of these differences and note that these differences need to be considered when interpreting time series of grid point comparisons.

4. How much is the difference between the simulated dust concentration from NAAPS and that from RAMS and WRF? I suggest the authors discuss this as they provide NAAPS dust concentration.

We agreed with reviewer 1 that inclusion of the NAAPS model snapshot does not offer much contribution to the paper since this is a comparison to an operational model and not real data. As such, we have removed the NAAPS figure panel and discussion from the paper.

5. How much is the expected uncertainty in your model values for radiative impacts?

There is not a general uncertainty that can be assigned to the radiation parameterization in the model. The RAMS radiation model physics predicts the radiative fluxes based on its radiative transfer equations that consider the presence of aerosols for this simulated event (Harrington 1997; Stokowski 2005).

6. I suggest comparing the radiative implications, such as radiative cooling/heating during

daytime and nighttime with observational data.

Observations of vertical profiles of radiative cooling/heating rates in and out of the dust plumes are not available. However, Stokowski (2005) demonstrated that RAMS is able to reasonably represent radiative heating associated with dust layers. Further, we have added discussion regarding the dust-induced changes in radiative fluxes and radiative heating/cooling and compared the RAMS simulated trends to those in Slingo et al. (2006) and Marsham et al. (2016). Both our results and those in the cited papers reveal a shortwave cooling trend at the surface due to dust as well as a counter balancing increase in radiative heating within the surface based dust layer. Both our results and the cited papers address the increase in radiative heating rates with respect to changes in the radiative flux divergence associated with attenuation of shortwave radiation by dense dust layers.

7. Refer to Figure 10f: Is this for Total LW fluxes? Or for total radiative fluxes (SW+LW)? Please check.

Figure 10 displays the mean profiles at night. As such, there are no shortwave contributions and only longwave fluxes are to be considered.

The Influence of Simulated Surface Dust Lofting and Atmospheric Loading on Radiative Forcing

Deleted: Erodible Fraction

Deleted:

Stephen M. Saleeby[1], Susan C. van den Heever[1], Jennie Bukowski[1], Annette L. Walker[2], Jeremy E. Solbrig[3], Samuel A. Atwood[1], Qijing Bian[1], Sonia M. Kreidenweis[1], Yi Wang[4], Jun Wang[4], Steven D. Miller[3]

[1]Department of Atmospheric Science, Colorado State University, Fort Collins, Colorado
[2]Naval Research Laboratory, Monterey, California
[3]Cooperative Institute for Research in the Atmosphere, Fort Collins, Colorado
[4]Department of Chemical and Biochemical Engineering, Interdisciplinary Graduate Program in Informatics, and Center for Global and Regional Environmental Research, University of Iowa, Iowa City, Iowa

Correspondence to: Stephen M. Saleeby (Stephen.Saleeby@colostate.edu)

Abstract. This high resolution numerical modeling study investigates the potential range of impact of surface-lofted dust aerosols on the mean radiative fluxes and temperature changes associated with a dust lofting episode over the Arabian Peninsula (2-5 August 2016). Assessing the potential for lofted dust to impact the radiation budget and temperature response in regions of the world that are prone to intense dust storms is important due to the impact of such temperature perturbations on thermally driven mesoscale circulations such as sea-breezes and convective outflows. As such, sensitivity simulations using various specifications of dust erodible fraction were performed using two high-resolution mesoscale models that use similar dust lofting physics based on threshold friction wind velocity and soil characteristics. The dust erodible fraction, which varies from 0.0 to 1.0 and controls the location and magnitude of surface dust flux, was varied for three experiments with each model. The "Idealized" experiments, which used an erodible fraction of 1.0 over all land grid cells, represent the upper limit on dust lofting within each modeling framework, the "Ginoux" experiments used a 1-degree resolution, spatially-varying erodible fraction dataset based on topographic depressions, and the "Walker" experiments used satellite-identified, 1-km resolution data with known lofting locations given an erodible fraction of 1.0. These simulations were compared to a "No-Dust" experiment in which no dust aerosols were permitted. The use of erodible fraction databases in the Ginoux and Walker simulations produced similar dust loading which was more realistic than that produced in the Idealized lofting simulations. Idealized lofting in this case study generated unrealistically large amounts of dust compared to observations of aerosol optical depth (AOD), due to the lack of locational constraints. Generally, the simulations with enhanced dust mass via surface lofting experienced reductions in daytime insolation due to aerosol scattering effects, as well as reductions in nighttime radiative cooling due to aerosol absorption effects. These radiative responses were magnified with increasing amounts of dust loading. In the Idealized simulation with "extreme" (AOD > 5) dust amounts, these radiative responses suppressed the diurnal temperature range. In the Ginoux and Walker simulations with "moderate" (AOD ~ 1-3) amounts of

Formatted: Font color: Text 1

Deleted: dust

Deleted: geographical

Deleted: case-study numerical

Deleted: provide

Deleted: s

Deleted: dust loading compared to

Deleted: i

Deleted: , non-spatially-constrained

Deleted: methods

Deleted: scenarios tends to

Deleted: of

Deleted: lead to

Deleted: simulation

Deleted: s

Deleted: concentrations

Deleted: effects

Deleted: noticeably

Deleted: model environment's

Deleted: lesser

lofted dust, the presence of dust still strongly impacted the radiative fluxes but only marginally modified the low-level temperature. Compared to the Ginoux simulation, the use of increased resolution in dust erodible fraction inventories in the Walker simulations led to enhanced fine-scale horizontal variability in lofted dust but only a modest increase in the mean dust concentration profile and radiative/thermal responses.

Deleted: is shown to

Deleted: while

Deleted: ying

Deleted: I

Deleted: are

Deleted: shown

Deleted: the

Deleted: details

Deleted: of dust lofting locations and potential, thereby, mitigate over-lofting and associated radiative response biases over regions that are unlikely source locations.

Deleted: ... [1]

1 Introduction

Dust aerosols are a substantial contributor to the global aerosol population, particularly in the dust belt region (Prospero et al. 2002; Tanaka and Chiba, 2006). They are known to strongly influence the radiation budget due to their significant scattering and absorption properties (Carlson and Benjamin, 1980; Haywood et al., 2003; Kinne et al., 2003; Sokolik and Toon, 1996; Dubovik et al., 2006). Dust aerosol layers can contribute to low-level atmospheric cooling due to the attenuation of shortwave radiation (solar dimming) through both scattering and absorption at solar wavelengths (Carlson and Caverly, 1977; Tegen and Lacis, 1996; Slingo et al., 2006; Lau and Kim, 2007; Kosmopoulos et al., 2017). Solar dimming can also lead to reduced surface heating, and thus, reduced latent and sensible heat fluxes (Wang et al., 2004; Prakash et al., 2015). In contrast, dust absorption of both longwave and shortwave radiation can contribute to localized heating by directly warming the dust-laden atmospheric layer and increasing downward thermal emission and by reducing the amount of surface thermal emission escaping to space (Tegen and Lacis, 1996; Slingo et al., 2006; Lau and Kim, 2007). A cooling tendency within a dust layer may also exist due to longwave emission, with a warming tendency adjacent to the dust layer (Slingo et al., 2006; Wang et al., 2013). The vertical distribution of dust also exerts a strong influence over surface and low-level radiative forcing and temperatures by modifying the vertical locations of solar scattering and radiative heating/cooling (Tegen and Lacis, 1996; Hsu et al., 2000; Slingo et al., 2006, Sokolik and Toon, 1996; Lau and Kim, 2007). A combination of the vertical distribution of dust, the overall aerosol loading, and the complex balance among shortwave scattering and absorption and longwave absorption and emission determines the net impact of dust on the low-level tropospheric temperature profile. As such, much uncertainty and variability remains among studies focused on the overall thermodynamic impact of dust storms with marked variability found on a case by case basis and with respect to varying observational and modeling platforms (Tegen and Lacis, 1996; Slingo et al., 2006; Prakash et al., 2015).

Deleted: complex

Deleted: the dust optical and radiative effects,

Deleted: and

Deleted: the

Through aerosol absorption and scattering processes associated with aerosol optical properties, lofted dust that is concentrated near the surface could potentially impact the lower atmospheric radiation budget sufficiently enough to alter the daytime and nighttime surface heating and low-level temperature profiles. Modification of the thermal profiles by dust loading has implications on the development of mesoscale weather features such as convection and sea-breezes whose circulations are driven or initiated by horizontal heterogeneities in local-scale thermal contrasts (e.g., Eager et al., 2008; Verma et al., 2006; Crosman and Horel, 2010; Ge et al., 2014). As such, it is necessary to improve our understanding of how dust lofted from Earth's surface can impact radiative quantities. Simulating dust lofting and its direct radiative effects via appropriate aerosol and radiation parameterizations within a numerical weather prediction model provides an effective way of elucidating the impacts of dust aerosols on the components of radiative and surface heating, and ultimately, their impact on low-level atmospheric temperature.

Numerical modeling of dust lofting requires a mechanical method of lofting dust from the surface dictated by the surface wind threshold friction velocity (Westphal et al., 1988; Marticorena and Bergametti, 1995). Dust lofting potential also varies with the soil type (Fecan et al., 1998) and vegetation (Pierre et al., 2012) and can be represented using geographical location datasets of dust erodible fraction that may vary dramatically in spatial coverage and resolution (Ginoux et al., 2001; Walker et al., 2009). The erodible fraction represents the percentage of surface soil that could potentially be mechanically lifted by the wind. Lofting by strong surface winds is favored in dry areas with bare, loose soil, and little to no vegetation. Inventories of dust erodible fraction (e.g. Ginoux et al., 2001; Walker et al., 2009) can be interfaced with dust lofting parameterizations to constrain the dust lofting potential over a given region.

Dust lofting occurs frequently over Saudi Arabia and along the Persian Gulf coastlines of the Arabian Peninsula (Tanaka and Chiba, 2006; Eager et al., 2008) and is maximized during the summer months (Prospero et al., 2002; Goudie and Middleton, 2006). Even though the Arabian Peninsula contributes substantially to the total lofted dust load in the northern Hemisphere (Tanaka and Chiba, 2006), few studies have focused on this region compared to the Sahara and east Asia (Prakash et al., 2015). Sea-breezes occur frequently along the Arabian Peninsula coastal zones, resulting from the intense heating of the land and strong land/sea temperature gradient (Verma et al., 2006; Eager et al., 2008), and dust lofting in this region is also maximized during the daytime due to enhanced local scale winds and turbulence associated with daytime heating (Middleton et al., 1986), as well as dust lofted by convective outflows (Miller et al., 2008). As such, this is a prime location for simulating and examining dust lofting in terms of its potential radiative impacts on the regional/local scale temperatures and associated forcing of mesoscale circulations.

This paper seeks to address research goals outlined by the Holistic Analysis of Aerosols in Littoral Environments (HAALE) team, a Multidisciplinary Research Program of the University Research Initiative (MURI) operating under auspices of Office of Naval Research (ONR). An overarching objective of the research is to identify the fundamental environmental factors that govern the spatial distribution and optical properties of littoral zone aerosols (including dust) at the sub-km scale. Within this scope, we hope to advance our understanding of aerosol direct and indirect impacts on the littoral zone meteorology, optical depth, and visibility and their associated feedbacks. As such, this paper seeks to first examine the predictability of dust generation and transport in models, and then, determine the influence of these predictions on the radiation budget in terms of feedbacks to the atmospheric thermodynamic structure, and thus, coastal mesoscale features such as sea-breezes. The HAALE team has chosen case studies that involve regions of intense aerosol production and transport that could interact with these littoral zone processes.

Numerical simulations were performed for a dust lofting event that occurred over the Arabian Peninsula from 2-5 August 2016. In this event, dust was lofted over this very arid region from multiple locations and multiple directions via strong surface winds. Simulations were performed using both the Regional Atmospheric Modeling System (RAMS) (Cotton et al., 2003; Saleeby and van den Heever, 2013) and the Weather Research and Forecasting Chemistry Model (WRF-Chem) (Skamarock et al., 2008; Grell et al., 2005; Fast et al., 2006). These two modeling frameworks were used to determine if there is a consistent and robust parameterization representation of dust emission and its impact on radiation parameters and temperature profiles. Within each model framework (RAMS and WRF-Chem), the analysis focuses on the following aspects: (1) the variability in lofted dust amounts from three different methods of specifying the dust surface erodible fraction, (2) the direct radiative impacts of the predicted dust lofting on the atmospheric and surface heating, and (3) the ultimate influence of these variations on the surface diurnal temperature cycle and atmospheric temperature profile.

The paper is outlined as follows: Sections 2.1 and 2.2 detail the RAMS and WRF-Chem model simulation designs and relevant parameterizations, respectively. Section 2.3 provides information on the three dust erodible fraction specifications being tested in this study. Section 2.4 describes the synoptic background setup for the 2-5 August 2016 Arabian Peninsula dust event. Section 3 provides simulated dust lofting and aerosol optical depth comparisons, and Section 4 details the dust radiative and temperature impacts. Section 5 concludes the paper with a summary of the main findings.

2 Model and Case Study Descriptions

2.1 RAMS Model Specifications

The RAMS model (Pielke et al., 1992; Cotton et al., 2003) version 6.2.06 was run over the Arabian Peninsula and surrounding region (Figure 1). This open-source version of RAMS is currently maintained by the research group of Prof. Susan C. van den Heever of the Department of Atmospheric Science at Colorado State University and can be found at the following URL: https://vandenheever.atmos.colostate.edu/vdhpage/rams.php. Initial RAMS simulations were run from 0000 UTC 2nd of August 2016 to 0000 UTC 5th of August 2016 on Grid-1 (15km grid spacing) (Fig. 1a). The 1-degree gridded Global Data Assimilation System Final Analysis (GDAS-FNL) data at 6-hour intervals were used to initialize and provide lateral boundary nudging for RAMS Grid-1. This parent grid (Grid-1) simulation was then used to generate the initial and boundary conditions for the Grid-2 simulations (2km grid spacing) run from 0000 UTC Aug 3 for 48 hours with model analyses available at 30 minute intervals (Fig. 1b). Both simulations were run with 50 terrain-following sigma-z vertical levels on a stretched grid with minimum vertical grid spacing of 75m near the surface. A summary of the RAMS model configuration and a general description of the physics packages used for simulations in this study are given in Table 1.

The RAMS double-moment microphysics parameterization module predicts the number concentration and mass mixing ratio of three liquid and five ice hydrometeor species (Walko et al., 1995; Meyers et al., 1997). Aerosol activation and cloud droplet nucleation are parameterized according to Saleeby and Cotton (2004) and Saleeby and van den Heever (2013).

Aerosol particles may be scavenged through nucleation and wet and dry deposition (Saleeby and van den Heever, 2013). Dust aerosols are mechanically lofted from the surface using the methods being tested herein (described below), and sea salt aerosols are generated over ocean surfaces under windy conditions as described in Saleeby and van den Heever (2013). Finally, an initial background pollution aerosol population was applied with a clean-continental profile containing 600 cm^{-3} at the surface and reduced exponentially aloft, similar to the clean-continental aerosol number concentration profile in Saleeby et al. (2016). All aerosol species can scatter and absorb shortwave and longwave radiation, thus, providing feedbacks to the dynamics and thermodynamics (Harrington, 1997; Stokowski, 2005). The refractive indices used across wavelengths for each aerosol species are shown in Stokowski (2005) and are guided by field data from the Saharan Dust Experiment (SHADE) (Haywood et al., 2003). For the radiative parameterization of dust species in RAMS an index of refraction of 1.53+0.0015i was used up to ~2000nm wavelength for building the optical lookup tables. The refractive index varied at longer wavelengths (Stokowski, 2005). Use of these values produced dust layer heating comparable to observations from SHADE (Stokowski, 2005).

Mechanical dust lofting in RAMS is a function of the threshold friction wind velocity (Marticorena and Bergametti, 1995), clay fraction of the soil (Fecan et al., 1998), and surface vegetation (Pierre et al., 2012). Low soil moisture, minimal vegetation, and strong winds provide optimal conditions for dust lofting. Dust lofting is internally computed for 7 particle radius bins (0.15, 0.26, 0.47, 0.83, 1.50, 2.65, and 4.71µm) (Tegen and Fung, 1994; Tegen and Lacis, 1996; Ginoux et al., 2001) which are then combined into 2 dust modes (sub-micron and super-micron) to minimize computational demands. Lofting is parameterized by dust particle size according to an inverse lofting relationship between aerosol size and threshold friction wind velocity (Alfaro and Gomes, 2001; Shao, 2001). Dust lofting is therefore ultimately computed in terms of dust mass flux as a function of particle size and the parameters discussed above, as well as the surface erodible fraction (Ginoux et al., 2001; Saleeby and van den Heever, 2013). The RAMS dust lofting parameterization is, thus, based on the Global Ozone Chemistry Aerosol Radiation and Transport Model (GOCART), with modifications to include combined dust size bins, soil clay fraction effects, vegetation influences, and variable erodible fraction specifications.

2.2 WRF-Chem Specifications

The WRF-Chem model version 3 (Skamarock et al., 2008; Grell et al., 2005; Fast et al., 2006), hereafter referred to just as “WRF”, was also used in this study to simulate the same dust lofting event over the Arabian Peninsula. WRF was run in a one-way nested grid configuration from 2-5 August 2016 with the outer Grid-1 at 15km horizontal spacing and inner Grid-2 at 3km spacing and 50 hybrid sigma-pressure levels. The WRF model domains cover nearly the same geographical area as the RAMS simulation domain shown in Fig. 1. WRF was run with the GOCART dust aerosol module (Ginoux et al., 2001), Morrison two-moment microphysics (Morrison et al., 2005,2009), specified aerosol optical properties (Barnard et al., 2010), RRTMG longwave radiation (Iacano et al., 2008), Goddard shortwave radiation (Chou and Suarez, 1999), NOAH land surface model (Niu et al., 2011; Yang et al., 2011), BMJ cumulus parameterization on the coarse grid domain (Janjic, 1994), and MYNN level 3 boundary layer parameterization (Nakanishi and Niino, 2006,2009). A summary of the WRF model configuration and a general description of the physics packages used for simulations in this study are given in Table 2.

2.3 Dust Erodible Fraction Experiments

This study uses the same relative dust lofting physics for each test simulation in both RAMS and WRF. The dust lofting in both models largely follow the GOCART methods from Ginoux et al. (2001). However, WRF retains dust in all lofted size bins while RAMS combines these into two bins, as mentioned previously.

Deleted: s

Deleted: of

Deleted: ,

Deleted: h

In the RAMS and WRF experiments, only the surface soil erodible fraction, which ranges from 0.0 to 1.0 (0% to 100% erodible), will be varied in the three methods that are now described. These erodible fractions are shown in Figure 2. The (1) “Idealized” method is similar to that used by Seigel and van den Heever (2012) in which an erodible fraction of 1.0 was used over their limited area model domain when simulating dust lofted by strong convection. Their study indicated lofted dust concentrations similar to those reported in severe dust storms over the southwest United States. The (2) “Ginoux” method uses the 1.0-degree global dataset of erodible fraction associated with Ginoux et al. (2001), which is shown in Fig. 2a, mapped to the Arabian Peninsula domains. The (3) “Walker” method uses a high resolution (~1.0 km) dataset of erodible fraction (Walker et al., 2009), which is shown in Fig. 2b mapped to the Arabian Peninsula domains. These three methods of specifying erodible fraction are described in further detail below.

Deleted:

The Idealized method represents the upper bound on potential dust lofting given that any grid cell in the domain with conditions that are favorable for dust lofting (strong wind, dry soil, bare soil, and favorable soil type) can indeed loft dust with an erodible fraction of 1.0. We suspect that the Idealized method, while useful for idealized simulations (e.g. Seigel and van den Heever, 2012), will produce extreme dust lofting in case study type simulations as are performed herein. However, it is useful to examine the upper bound of lofted dust that could be expected within a given case study and modeling framework. The Walker database erodible dust locations were identified manually using satellite data, and thus, this database identifies specific locations at approximately 1km resolution where dust is known to be available for lofting. Known dust locations in the Walker database are designated with an erodible fraction of 1.0. The Ginoux database identifies more expansive dust lofting areas, compared to the Walker database, but with lower erodible fractions. The Ginoux database is based on the fraction of erodible sediment associated with topographic depressions as used in the GOCART model. The analysis that follows will refer to these three varying methods of assigning dust erodible fraction using the terms “Idealized”, “Ginoux” and “Walker”, and it will compare the varying amounts and locations of dust that is lofted according to these different specifications of erodible fraction. Further, simulations were also run without dust lofting, denoted as “No-Dust”, to provide a baseline comparison against simulations lofting dust. A summary of these simulations is provided in Table 3.

Deleted: The Ginoux database identifies broader dust lofting areas with lower erodible fractions than the Walker database.

Deleted:

Deleted: based on observations

Deleted: ;

Deleted: k

While sea salt was generated in these simulations and initial pollution aerosols are present in RAMS, and while WRF continues to generate a variety of aerosol species, the amounts of these aerosols are relatively small compared to the amounts of dust generated in all of these case study simulations. As such, this analysis will focus largely on the dust aerosols, with specific emphasis on the varying amounts of dust emitted to the atmosphere and its subsequent influence on the radiation and surface energy budget and temperature profile as a result of the dust erodible fractions being utilized.

It is important to note that the goal of the current analysis is to determine the sensitivity of the radiation budget and thermal response, within each modeling framework (RAMS and WRF), to the presence of lofted dust that varies with the geographical specification of dust erodible fraction. It is not the intent of this study to examine and interpret the modeling differences arising due to the model frameworks being utilized (i.e., RAMS vs. WRF). As such, differences in the model setup and parameterizations (with the exception of the dust lofting parameterizations) are not being considered within the scope of this investigation.

2.4 Case Study Description

The dust lofting event simulated herein occurred from 2-5 August 2016 over the Arabian Peninsula with primary lofting occurring from (1) northerly flow over central Saudi Arabia and (2) southerly flow from coastal Oman to the United Arab Emirates (UAE) (Figure 3). For the duration of this event, there is large scale high pressure and anti-cyclonic flow aloft over the Arabian Peninsula as inferred from the GDAS-FNL 500mb heights on 0000 UTC 4 August 2016 (Fig. 3a). This analysis time is 48 hours into the RAMS and WRF simulation times on the parent Grid-1, 24 hours into the simulations on the high-resolution Grid-2, and is just prior to the model analyses of instantaneous vertical profiles of radiative and thermal fields to be discussed in the sections that follow.

The GDAS-FNL streamlines at 925mb display the near surface flow that impacts dust lofting (Fig. 3b). The 00Z August 4, 2016 streamline analysis exhibits cyclonic flow over the southern Persian Gulf. There is northerly flow over central Saudi Arabia that leads to a large dust source in that region being transported southward as seen in the Moderate-resolution Imaging Spectro-radiometer (MODIS) Aqua satellite image (Figure 4a). The southerly to southwesterly flow over Oman and the eastern Rub al Khali mobilizes regional dust sources. Dust lofted in this area is transported to the northeast toward the UAE where additional mobilized dust is added from local sources. The wind field then transports the lofted dust in the southeasterly flow over the Persian Gulf where the mineral aerosols become quite evident as a highly visible plume over the Persian Gulf by 0930 UTC Aug 4 (Fig. 4). Due to the similar coloration between the dust mass and land mass in the visible imagery, the dust plumes over the Arabian land area are difficult to distinguish from the background. MODIS retrieved AOD associated with the lofted dust is shown in figure 7 for two satellite overpasses during this event. The retrievals reveal substantial amounts of dust associated with plumes over both Saudi Arabia and the Persian Gulf. The MODIS AOD retrievals are discussed in further detail in section 3.1.

Deleted: a

Conditions are very warm over the land regions at this time, as seen in the GDAS-FNL 1000mb temperature field (Fig. 3c) with temperatures exceeding 44°C in some locations. The equivalent RAMS and WRF simulated fields of 500mb heights, 925mb streamlines, and 1000mb temperature from the Walker simulation on Grid-1 are shown in Figs. 3d-f and Figs. 3g-i, respectively. The modeled geopotential height fields both indicate broad scale high pressure similar to the GDAS data. The modeled streamlines also depict the strong northerly flow over Saudi Arabia and onshore southerly flow over Oman and Yemen associated with the two main dust plumes. The model simulated 1000mb temperatures tend to be 2-4°C higher over the Saudi interior in both models. Differences in topography and land-surface parameterizations may account for the discrepancies in the magnitude of predicted temperature between the reanalysis and the RAMS and WRF simulations, while the differences in fine scale horizontal variability are likely the result of differences in grid resolution between the reanalysis and model simulations. Though not shown, near-surface humidity is low and soils are very dry and conducive to dust lofting, with mean volumetric soil moisture values between 0.04-0.05 m^3 m^{-3}.

3 Dust Lofting and AOD Comparisons

To obtain a first glimpse of the differences in the amount of dust generated via the various dust lofting erodible fraction assumptions, the total dust mass at the lowest model level (36m) in RAMS and near the surface (945hPa) in WRF at 0930 UTC 4 Aug is shown in Figure 5. This is the same time as the satellite image in Fig. 4. It can be seen that the Idealized method in RAMS (Fig. 5a), used by Seigel and van den Heever (2012), produces an extraordinary amount of dust compared to the simulations using constrained lofting locations and erodible fraction. The Idealized method appeared to perform well for the short-term, idealized Seigel and van den Heever (2012) study, but it does not appear to produce realistic results for a lengthier simulated case study environment. The Idealized WRF simulation also produces very unrealistically high values of dust in many areas of the domain (Fig. 5d). As mentioned earlier, the Idealized simulations are representative of an upper bound on lofted dust that can be generated within a given modeling framework. As such, the thermodynamic and radiative effects of dust, to be discussed, in the Idealized dust lofting scenario represent an upper bound on the dust-related feedbacks.

The Ginoux and Walker database applications are surprisingly similar in their dust amounts and locations in RAMS (Fig. 5b,c) and in WRF (Fig. 5e,f). In both models, the Walker simulation produces more fine-scale spatial variability with respect to the lofting locations due to the precise, high resolution nature of the database. It also leads to greater amounts of near-surface dust mass in some locations, such as central Saudi Arabia, southeast Oman and northwest Oman, since the erodible fractions in these areas are not as diffuse as in the coarser Ginoux data. It should be noted that while the Walker database leads to greater spatial variability in simulated lofted dust, this does not imply that the Walker simulations are more accurate than the Ginoux simulations with respect to the net amount of lofted dust across the model domains. Walker et al. (2009) provide a quantitative assessment of the use of high-resolution point source dust locations.

In sections 3.1 and 3.2 that follow, we present AOD estimates from two MODIS overpasses and two AERONET stations

Deleted: se

Deleted: fields in both models compare favorably to the gridded analyses, though,

Deleted: s

Deleted: models

Deleted: predicted temperature.

Deleted: ... [2]

Deleted: The Navy Aerosol Analysis Prediction System (NAAPS) model surface dust image from 0600 UTC Aug 4 (Fig. 4b), around the time of the MODIS image shown in Fig. 4a, indicates surface dust concentrations that are quite high and maximized over: (1) the central Arabian Peninsula in association with the large scale northerly winds over that region and (2) the coastal zones of Oman and Yemen, and (3) the UAE and the southern end of the Persian Gulf in association with the strong southerly flow. The NAAPS image does not show the dust plume feature over the Persian Gulf that is evident in the MODIS imagery. This may be due to the fact that only surface dust concentrations are being displayed in the NAAPS output.

Deleted: a

Deleted:

Deleted: captures more dust mass detail that were available within the domain during this dust event. Given the sparsity of the MODIS and AERONET data available during this event and the limited coverage over the model domain, the comparisons with the simulated AOD are made in a qualitative manner. Our intent is to broadly demonstrate that the RAMS Ginoux and Walker simulations were able to generate the Saudi and UAE dust plumes at the approximate location and of similar AOD compared to the limited dust observations. From there, we focus on examining the potential range of radiative effects of the Saudi dust plume simulated with varying specifications of dust erodible fraction which lead to varying amounts of lofted dust.

3.1 MODIS vs. MODEL AOD

The RAMS total aerosol optical depth (AOD) at 550nm wavelength was computed offline via RAMS aerosol output. This output is, as expected, highly dominated by the dust modes. Aerosol particles were first grown hygroscopically to equilibrium with model relative humidity in each grid box using κ-Köhler theory (Petters and Kreidenweis, 2007). Aerosol extinction, and thus, AOD, is a function of the real part of the index of refraction. A representative real refractive index for dust of 1.53 at 550nm was assigned based on surface observations (such as AERONET) (Dubovik et al., 2006; Giles et al., 2012), radiative closure studies (Wang et al., 2003; Christopher and Wang, 2003), and laboratory studies (Di Biagio et al. 2019). This value matches that used in the RAMS parameterization of dust radiative effects. Refractive indices for hygroscopic species were adjusted based on volume mixing with water. Representative extinction coefficients for each model grid box were then calculated for each aerosol species using Mie theory (Bohren and Huffman, 1983). AOD in each 2-D model column was then calculated for each species using the extinction coefficients and heights in each column grid box and then summed for all aerosol species to produce an estimated total AOD. The WRF AOD is computed via Mie theory during runtime and is output as a standard 2D quantity. Similar to RAMS, a real refractive index of 1.53 for dust was used in WRF for generating AOD at 550nm wavelength.

The 550nm AOD at 0930 UTC 4 Aug for each of the RAMS and WRF test simulations is shown in Figure 6. The figure panels coincide with the same panels of dust concentration from Fig. 5 for the same time. Maxima in AOD tend to coordinate with the maxima in near-surface dust concentration. AOD for the Idealized case is unrealistically high in both RAMS and WRF as expected from the extreme near-surface concentrations of dust (Fig. 5a,d). The RAMS Ginoux and Walker dust simulations indicate dust plume AOD values in the 1.5-2.5 range associated with the UAE and central Saudi dust plumes. The RAMS Ginoux simulation generates a plume over the UAE and Persian Gulf that is more expansive than that in the Walker simulation, though maximum AOD values are less than in the Walker generated plume. This is perhaps not unexpected given that the Ginoux dust sources cover a relatively larger area but with lower erodible fraction. The Saudi dust plume in the Walker simulation is both more expansive and contains higher maximum AOD at the time shown. This could also be expected given the relatively high density of dust sources in the Walker database in this area and the relatively low erodible fraction in the Ginoux database over central Saudi Arabia (see figure 2). The Ginoux and Walker simulations from WRF also show the relatively highest AODs associated with the Saudi dust plume and the UAE dust plume. However,

Deleted: The snapshot of NAAPS surface dust concentration (Fig. 4b) displays notable similarities in the locations of the dust maxima and in the maximum concentrations despite differences between the NAAPS analysis (in time and vertical location) and the simulations performed herein.

Deleted: of

Deleted: (

Deleted: 50

Deleted: +0.005i)

Deleted: using methods that adopt an imaginary spheroid-like index of refraction for non-spherical dust as revealed by

Deleted: and

Deleted: This allows for application of Mie theory to determine scattering, absorption, and AOD.

Deleted: maximum

Deleted: 2.0-3.0

dust plume AOD values from WRF (0.5-1.0) tend to be noticeably lower than those from RAMS (1.5-2.5) at the time shown. The lower AOD in WRF compared to RAMS results from much less generation of lofted dust in WRF (Fig. 5).

The MODIS Aqua and Terra 550nm AOD at 10km resolution (mapped to the RAMS 2km domain) at approximately the same time are shown in Figure 7a,b. These MODIS-based AOD retrievals are obtained from MODIS Collection 6 product and are further processed with retrievals over the coastal turbid water (Wang et al., 2017); they have an uncertainty of ~15-20% over land and 10% over ocean (Levy et al., 2013; Hsu et al., 2013; Wang et al., 2017) and may over-estimate AOD in situations of high dust loading (Remer et al., 2005). The MODIS data shown represent the two overpasses available during this case that have the least amount of missing data from the retrieval.

Similar to the RAMS Ginoux and Walker simulations, the MODIS AOD values in the dust plumes over the UAE, Oman, and Saudi Arabia are also in the 1.5-2.5 range with some pixels perhaps indicating even higher values over the Persian Gulf. The RAMS Ginoux and Walker simulations are, thus, performing favorably with respect to generating amounts of lofted dust that lead to AODs that are similar in magnitude to the limited remote sensing observations of the two main dust plumes. A visual comparison of the dust plumes among the MODIS visible image, MODIS AOD retrievals, and model AOD indicate that the RAMS simulated plumes are slightly displaced, with the Saudi plume located slightly north of the observed location and the UAE plume not extending as far north into the Persian Gulf as that observed. We also note that these simulations generate a more distinct gap of lower AOD between the two plumes. While variability in the transport of the dust plumes in the RAMS simulations leads to some discrepancy in the plume placement, both the RAMS Ginoux and Walker simulations produce dust plumes that are similar in expanse and AOD to those shown in the MODIS AOD. As such, an investigation of the impacts of locally lofted dust in these simulations may offer insight into the potential radiative and thermal response across a range of realistically simulated dust plumes that vary due to differences in dust erodible fraction.

Both RAMS and WRF generate the two key dust plumes from surface lofting over central Saudi Arabia, Oman and the UAE, with RAMS producing dust plume AODs in the Ginoux and Walker simulations that reflect the AOD values from the limited observations. Results from the Idealized simulations from both models indicate the need for application of dust source databases to dust lofting schemes, while simultaneously demonstrating the anticipated upper range of potential dust lofting within each given model framework. For the sake of brevity, and given that WRF tends to under-predict dust plume AOD in the Ginoux and Walker simulations, the remainder of this manuscript will now focus only on results from the RAMS simulations. A more extensive model inter-comparison needed to understand the differences in dust mass and AOD between RAMS and WRF is left for future investigation. Given that both models use the lofting techniques of GOCART and the same erodible fraction databases, we speculate that the prediction of the near-surface wind speed, soil moisture, dust deposition, and dust binning techniques may all play a role in explaining the difference in amounts of simulated lofted dust.

Deleted: .

Deleted: Maximum

Deleted: Persian Gulf

Deleted: 2.0-3.0

Deleted: There is also a large area with AODs in the 1.0-2.0 range present over Saudi Arabia, UAE, and Oman in both the MODIS AOD and in the RAMS Ginoux and Walker simulations. This suggests the

Deleted: RAMS

Deleted: model is

Deleted: appropriate

Deleted: in space and

Deleted:

Deleted: that are available when using either the Ginoux or Walker databases with RAMS

Deleted: The Ginoux and Walker simulations from WRF also show the relatively highest AODs associated with the central Saudi dust plume and the UAE/Persian Gulf dust plume; however, WRF AODs are lower (0.5-1.0) than the RAMS values in the plume regions due to less generation of lofted dust compared to RAMS.

Deleted: display similar predicted synoptic situations which indicate good conditions for wind induced

Deleted: generated

Deleted: The trends in dust lofting resulting from differences in the application of dust erodible fraction datasets are also similar between RAMS and WRF, which emphasizes the

Deleted: usefulness of high resolution dust databases in numerical modeling of dust lofting and transport. As such, and for

3.2 AERONET vs. RAMS AOD

The time series of AOD (at 500nm) from the Aerosol Robotic Network (AERONET) (Holben et al., 1998,2001; Smirnov et al., 2002) from the Mezaira, UAE site (level 1.5 data) (Fig. 7c) and Kuwait University, Kuwait site (level 1.0 data) (Fig. 7d) are shown along with the associated RAMS total AOD (at 550nm) time series for the corresponding grid point locations. The locations of these two sites are indicated by the large black dots in Fig. 7a,b. AERONET data are only available during daylight hours. At the Mezaira site, the simulated AOD for the Mezaira grid point location most closely agrees with the AERONET AOD in the Ginoux and Walker simulations. The No-Dust simulation demonstrates the substantial contribution that dust, when included in the simulations, makes to the total AOD. The excessively high AOD in the Idealized simulation indicates that constraints on the erodible fraction are necessary to generate a reasonable prediction of both dust mass and AOD. Both the Ginoux and Walker simulations appear to underestimate the AERONET AOD at the Mezaira grid point. However, both simulations show an increase in AOD from Aug 3 to Aug 4 as in seen in the observations. As noted earlier, the RAMS simulated dust plumes are slightly displaced compared to the plumes seen in the MODIS data. Caution should be exercised when making single grid point comparisons like these as they can be deceiving when key model features are shifted within the simulations. The Walker AOD time series at Mezaira remains relatively low since the dense part of the plume is shifted a bit to the east and the Mezaira grid point in the model sits within the gap region between the plumes. The Ginoux dust plume is broader than the Walker plume due to the widespread nature of the dust source locations in the region as discussed earlier. As such, the Ginoux AOD time series displays higher AOD than the Walker simulation, and more closely compares to the AERONET AOD at Mezaira during the dust plume passage.

To demonstrate the range of spatial variability in simulated AOD and the need to consider plume displacement, the time series of AOD in the Ginoux and Walker simulations for the grid point 2-degrees to the east of Mezaira are shown as the colored, dotted lines in Fig. 7c. This location to the east of Mezaira is more clearly in the simulated dust plume, with the Ginoux simulation matching well with the Mezaira AERONET, while the Walker simulation produces higher AOD that perhaps represents the maximum aerosol concentrations within this plume. As such, where the plume is sampled and where the model places the plume in the simulations greatly impacts the comparison to individual grid point observations.

The MODIS AOD values are also interpolated to the Mezaira AERONET location as shown by the large blue and orange dots on figure 7c. For the two given overpasses the MODIS grid point estimates are lower than the AERONET AOD. While part of the difference could be attributed to uncertainty in AOD from MODIS and AERONET data for high AOD conditions, the horizontal interpolation of the MODIS pixels to the Mezaira point location occurs in an area with gradients in AOD and near missing data pixels. As such, the interpolations likely reduce the MODIS AOD grid point estimates at Mezaira. However, both the MODIS and AERONET AOD data indicate the presence of a substantial dust plume that is well above the background state seen at the beginning of the time series in figure 7a.

Deleted: measured

Deleted: s

Moved down [1]: Caution should be exercised when making grid point comparisons like these as they can potentially be deceiving if key synoptic and mesoscale flow regimes are slightly shifted in one direction or another within the simulations.

Moved (insertion) [1]

Deleted: potentially

Deleted: if key synoptic and mesoscale flow regimes are slightly

Deleted: in one direction or another

Deleted: T

Deleted: e

Deleted:

The northern Kuwait University AERONET site is well removed from the intense dust episodes and is located in an area with only small horizontal AOD gradients indicated in the model output. The AOD values vary from ~0.2-0.7 on Aug 3 and from ~0.3-0.5 on Aug 4. The Ginoux and Walker simulations indicate very similar AOD predictions with values from 0.2-0.7 during this two-day time frame. This AERONET site is clearly not being impacted by dust plumes during this time. Kokkalis et al. (2018) examined a decade of AERONET data at this Kuwait City location and found mean daily AOD values of 0.45±0.29, which is similar to the AERONET and RAMS model AOD during this event (Fig 7d). They also identify dust storm mean AODs as having values of 1.04±0.32 with some larger events exceeding an AOD of 1.5. This is rather representative of what is seen in the Mezaira AERONET and simulated UAE dust plumes. The largest contributor of dust storms to this location originate from Saudi Arabia. While the timing of the simulated AOD maxima and minima do vary slightly from the AERONET observations at the Kuwait site, the overall prediction is quite reasonable given the inherent difficulty in accurately simulating all of the variables that feed into prognostic dust lofting and its transport and removal mechanisms.

It should be noted that the Mezaira site is located between the central Saudi Arabian dust maximum and the dust plume over Oman and eastern UAE, as can be seen in the satellite imagery and model output. Since the Ginoux and Walker simulations appear to offer a reasonable prognosis of dust lofting and transport, one might expect observed AOD values as high as 2.5-3.0 in the nearby dust plume in the eastern UAE. Given the significant spatial and temporal variability in dust amounts, this is an area of the world that could significantly benefit from additional AERONET stations that could assist with model initialization and/or validation of major dust events. This would also help to determine if model simulations of AOD magnitudes are reasonable but could use improvement regarding the placement of specific dust storm events.

4 Dust Impacts on Radiation

For the remainder of the discussion, the analyses of the model output will focus on the direct radiative effects of dust in the RAMS model, how these effects vary among the three simulations with various dust erodible fractions, and how this ultimately impacts the temperature profiles over significantly dusty arid regions. To isolate the specific dust effects on radiation over this simulated domain that includes flatlands, mountainous terrain, coastal zones, and ocean area, we examined an inland area over the central Saudi Peninsula where dust concentrations are rather high and cloud cover was minimal. This sample region was chosen so as to exclude from the analysis any potential variability in cloud cover and maritime influences among simulations. Time series and vertical profiles of several quantities will be presented as area averages within the 5°x5° box that is denoted in Fig. 1b. Instantaneous vertical profiles will be shown for nighttime at 0200 UTC (~0600 LST) and for daytime at 1000 UTC (~1400 LST) on the 4th of August 2016. These times were chosen since they represent the approximate times of the peaks in nighttime cooling and daytime heating, respectively.

4.1 Dust and Temperature Time Series

To begin, Figure 8a depicts the time series of horizontally averaged integrated dust mass over the analysis box region (Fig. 1b) from the high-resolution RAMS model domain. From this perspective, the Ginoux and Walker databases give very similar results, with the Walker database leading to slightly greater dust amounts, likely due to the localized dust lofting areas with high erodible fraction over central Saudi Arabia, southeast Oman and northwest Oman (see Figs. 2b and 5c). The Idealized dust simulation produces dramatically greater dust amounts that generally continue increasing over time as a result of lofting rates exceeding deposition rates. Some of the radiation and temperature responses to the dust evolve over time as the model domain transitions from a cleaner to dustier environment. As such, the focus of the analysis will largely be on day-2 (0000 UTC Aug 4 to 0000 UTC Aug 5). However, some linkage can be made to the model state on day-1 (Aug 3), which is displayed in the time series for completeness. For the remainder of the manuscript, the Idealized dust case is periodically referred to as containing an "extreme" dust amount while the Ginoux and Walker cases will be referred to as those with "moderate" dust amounts.

The time series of near-surface temperature (Fig. 8b) reveals a couple of key patterns that arise by day 2. The minimum nighttime near-surface temperature tends to increase with increasing dust amount while the maximum daytime temperature is lowest for the extreme dust amounts in the Idealized case and highest for the moderate dust amounts in the Ginoux and Walker cases. The greater near-surface daytime temperature in the moderate dust cases is only slightly greater than the No-Dust control case, while the temperature reduction of ~3°C in the Idealized case is comparatively large. In general, very large amounts of lofted dust tend to reduce the overall near-surface diurnal temperature range. Moderate amounts tend to have variable impacts on the diurnal near-surface temperature cycle. The analyses that follow will attempt to identify which radiative components impact these noticeable changes in nighttime and daytime temperature extremes.

4.2 Daytime Radiative Fluxes

This section examines daytime (1000 UTC, ~1400 LST for 4 August) vertical profiles of quantities averaged over the analysis box region discussed earlier. This daytime snapshot is taken around the time of maximum: (1) downward shortwave radiation (Fig. 8c), (2) upward longwave radiation (Fig. 8d), (3) surface sensible and latent heat fluxes (Fig. 8e,f), and (4) near-surface temperature (Fig. 8b). There is some time lag between maxima in radiation, surface fluxes, and temperature, but they tend to occur within about an hour of one another in this case. Vertical profiles of dust concentration in figure 9a indicate the lowest dust concentrations from the Ginoux simulation, slightly greater values from the Walker simulation and substantially high concentrations for the Idealized simulation. While the Ginoux and Walker simulations have very similar amounts of lofted dust, the Walker simulation likely produces greater amounts of dust due to a relatively large number of source locations over the analysis region and comparatively low erodible fractions in the region from the Ginoux database (see figure 2).

Of the radiative quantities examined, the daytime surface downward shortwave radiation (Figure 9f) is the radiative flux that is most greatly impacted by dust, which is in keeping with previous findings (e.g. Slingo et al., 2006; Marsham et al. 2016). Scattering and absorption of dust at solar wavelengths tends to reduce the amount of shortwave radiation penetrating downward through the atmosphere. This impact is found to be greatest near the surface, which corresponds to increasing dust amounts near the ground (Fig. 9a). The downward shortwave profile shows reductions from 200-800 W m^{-2} that scales with the trend in average dust amounts. The shortwave reductions by dust of ~200-250 Wm^{-2} for the Ginoux and Walker simulations are similar to those shown by Slingo et al. (2006) and Kosmopoulos et al. (2017) for corresponding dust AOD in the range of 1.5-2.5. These reductions by themselves would tend to induce a cooling effect near the ground during the daytime by limiting the land surface heating. This effect is manifest in Fig. 8, which shows that the daytime surface sensible (Fig. 8e) and latent heat (Fig. 8f) fluxes are also reduced under conditions of greater dust loading. The daytime surface upward longwave radiation (Fig. 8d) is also reduced with increasing dust and decreasing surface insolation since the ground is heated less effectively and emission temperatures are lower. Again, the most noticeable impacts are on day-2 in association with the greater lofted dust amounts (Fig. 8a).

Formatted: Superscript

Deleted: s

The ultimate impact of dust on the temperature profile is determined by a complex balance between upward and downward short and longwave radiative fluxes (Fig. 9), as well as ground heat storage and surface sensible (Fig. 8e) and latent (Fig. 8f) heat fluxes that regulate the boundary layer processes and, thereby, the dust vertical profiles in the boundary layer. Marsham et al. (2016) also highlight the complex balance of radiative fluxes in determining the net radiative response to dust loading. The ability of dust to scatter and absorb shortwave radiation (e.g. Banks et al. 2014; Marsham et al. 2016) and absorb and emit longwave radiation (e.g. Haywood et al. 2005; Marsham et al. 2016) influences these fluxes, thus impacting the temperature profile. While the downward shortwave response to dust is rather straightforward, the other fluxes are more variable and trends are less monotonic. The upward shortwave (Fig. 9g) response to dust follows the downward shortwave trend since surface albedos are similar among experiments. The downward longwave flux (Fig. 9d) in the lowest 3km, where most of the dust resides, corresponds to downward re-emission of radiation absorbed by dust. As such, this shows a trend of greater downward longwave flux with an increase in dust mass in the lowest several kilometers. The upward longwave flux (Fig. 9e) displays only small differences near the ground for the moderate dust amounts, but decreases under extreme dust loading. The noticeable decrease in upward longwave flux in the extreme dust lofting case results from cooler surface temperatures (Fig. 8b and 9c), and thus, lower thermal emission rates. The increase in downward longwave emission in the dust layer, which partially offsets the cooling effect of reduced shortwave at the surface, has also been noted in observational studies (e.g. Slingo et al., 2006; Hansell et al., 2010; Marsham et al., 2016). Generally, the changes in fluxes from the No-Dust case increase with increasing dust amount from the Ginoux to Walker to Idealized dust simulations. However, the differences between the Ginoux and Walker simulated fluxes are smaller compared to those from the Idealized simulation due to similar dust loading.

The total or net radiative flux (downward minus upward sum of shortwave and longwave fluxes) tells a more concise story of the atmospheric radiative impacts of dust (Fig. 9h). Near the surface there is a monotonic trend of decreasing total radiative flux that trends with increasing dust mass from the Ginoux to Walker to Idealized dust simulations. A decrease in surface net radiative flux with increase in dust loading was also found by Marsham et al. (2016). Similar to the RAMS simulation results, Marsham et al. (2016) revealed that the dust-induced reduction in surface shortwave heating is greater than the corresponding increase in longwave heating, with a resulting reduction in net radiative fluxes. By itself, the difference in the magnitudes of the total radiative flux among the various dust mass conditions suggests that, near the surface, the presence of dust should induce a cooling effect. Above the surface, the total flux increases with height, with the rate of increase (the slopes) being steeper for greater dust mass. The profiles increase within the dusty layers and then assume a neutral slope aloft that is similar to the No-Dust scenario. Above ~6km AGL the comparative total radiative flux profiles show a monotonic increase with increasing low-level dust mass – a trend that is opposite to that of the near-surface. This behavior is due to the steepness of total flux profiles within the dust layers. A more positive value of total radiative flux corresponds to greater atmospheric accumulation of short and longwave radiation, and thus the potential for greater warming. The trend in total radiative flux above ~6km suggests that low-level dust layers can induce a net warming effect in the column above them.

In addition to the magnitude of the total radiative flux, the radiative flux divergence or radiative heating rates, also contribute to atmospheric heating and cooling associated with dust layers. The slopes of the total radiative flux profiles are indicative of the magnitude of the radiative flux divergence. The slopes are steeper for greater dust mass, which indicates greater radiative flux divergence within the dusty layers and stronger radiative heating rates. The associated radiative heating rate profiles (Fig. 9b) indicate a strong atmospheric radiative heating impact of dust from ~7km to the surface that increases monotonically with increasing dust mass from the Ginoux to Walker to Idealized dust simulations. Observations have also shown increases in radiative heating rates with dust loading associated with increases in radiative flux divergence within the dust layers (e.g. Hansell et al., 2010; Marsham et al., 2016). The cooling effect of reduced surface net radiative fluxes can be countered by an increase in radiative heating within dust layers.

The resulting atmospheric temperature profile is thus controlled by a complex interaction among the: (1) magnitude of total radiative fluxes, (2) radiative flux divergence / radiative heating rates, (3) surface latent and sensible heat fluxes, and (4) atmospheric mixing. The area-mean low-level maximum daytime temperature profile (Fig. 9c) indicates a dust induced heating effect above ~600m AGL, below which, there is a cooling effect imposed by extreme dust loading. In the lowest 200m or so, the extreme dust loading has reduced the daytime mean maximum temperature by about 2.5°C. The moderate dust amounts lead to a small warming of about 0.3-0.4°C near the ground despite reduced total radiation and reduced sensible and latent heat fluxes. This warming, which is only slightly more in the Walker simulation compared to the Ginoux simulation, appears to be induced by the increased net radiative heating rates shown in (Fig. 9b). Thus, except for the case of

Deleted:

extreme dust loading, lofted dust tends to induce a net warming effect at the surface despite reductions to insolation. We suspect that in our simulations, the weighting of dust toward the surface prevents substantial surface cooling except in the presence of very high and unrealistic dust loading. The in-layer atmospheric radiative heating rates counter balance the surface cooling effect of dust. Had the dust been concentrated in an elevated layer, we may expect to see a stronger and more consistent surface cooling during the daytime with the radiative heating rates concentrated in the dust layer aloft (e.g. Lau and Kim, 2007; Shell et al. 2007).

4.3 Nighttime Radiative Fluxes

This section examines nighttime (0200 UTC, ~0600 LST for 4 August) vertical profiles of quantities averaged over the analysis box region discussed earlier. At nighttime, the radiation and associated temperature responses behave differently compared to the daytime. Over the nighttime hours, the solar component of radiation is no longer a factor (Fig. 8c). The surface upward longwave radiation trends (Fig. 8d), however, indicate a clear maximum increase of nearly 50 Wm^{-2} between the no-dust and extreme dust case in the pre-dawn hours of 4 August. Further, the overnight near-surface temperatures (Fig. 8b) are monotonically warmer in the dusty cases with a maximum difference just before dawn. The latent and sensible heat fluxes are relatively small at night (Fig. 8e.f), although there is a modest increase in the nighttime latent heat flux with dust loading that could be contributing to warmer near-surface temperature. Though not shown, this stronger latent heat flux under warmer, dustier conditions may result from modestly stronger winds that occur in association with warmer temperatures and more boundary layer mixing.

The near-surface temperature and upward longwave radiation discussed above are not quantities that are independent of one another, but rather, one largely determines the other. As such, a closer examination of the nighttime radiation vertical profiles in the hour just before dawn demonstrates the key controlling factors that impact the nighttime temperature response to dust loading.

First, the nighttime vertical dust concentration profile (Figure 10a) is very similar to the daytime profile with dust concentrations increasing from the Ginoux to Walker to Idealized simulations (Fig. 9a). The nighttime temperature profile responds variably to dust loading between the near-surface layer and layers aloft in the moderate dust cases, but is consistently warmer from the surface upward in the extreme dust case (Fig. 10c). Right near the surface, there is a monotonic increase in temperature with dust loading. The extreme dust event shows a temperature increase of ~3°C compared to the No-dust case while the moderate dust events indicate increases of ~1°C for the Walker simulation and ~0.5°C for the Ginoux simulation. The increase in near-surface temperature occurs in the moderate dust cases despite stronger radiative cooling rates (Fig. 10b) in those cases compared to no-dust. This results from a comparatively smaller total radiative flux (less negative) near the ground (Fig. 10f), which implies reduced longwave emission. The slightly greater surface latent heat fluxes in the dusty simulations also enhance near-surface warming. As such, near the surface, the increase in latent heat flux

Deleted: over

Deleted: no

and reduction in net thermal emission appear to play a greater role towards a warming effect of dust than the opposing stronger radiative cooling rates in determining the nighttime near-surface temperature warming trend with dust loading.

Above the first few hundred meters, however, the temperature trend is non-monotonic and the moderate dust cases indicate a minor cooling impact of ~1°C. The downward longwave flux profile (Fig. 10d) shows a monotonic trend that increases with dust loading below ~3km AGL with a maximum increase of over 100 Wm^{-2}; this increase is associated with the dust layer absorbing thermal radiation and re-emitting this back towards the ground (e.g. Slingo et al., 2006; Marsham et al. 2016). The upward longwave (Fig. 10e) trend is monotonic right near the surface, similar to what is seen in the associated upward longwave time series (Fig. 8d). Above 3km, however, the moderate dust cases display slightly greater upward longwave fluxes compared to No-Dust, while the extreme dust case is consistently less than the No-Dust and moderate dust cases. The non-monotonic trend in the upward longwave results from a competition between the upward thermal emission near the top of main dust layer and the amount of thermal radiation which is absorbed by the dust. The reduction in upward longwave in the extreme dust case is rather large and results from dust absorption of thermal radiation and warming of the layer, which prevents less longwave escaping to space. This effect is less substantial in the moderate dust cases, thus leading to a non-monotonic response in upwelling longwave radiation to an increase in dust mass.

The total radiative flux (Fig. 10f) below 1km is monotonically reduced (less negative) with increasing dust concentration from the Ginoux to Walker to Idealized simulation which suggests a near-surface warming effect. Above ~1km AGL, however, the total flux trend is non-monotonic. Moderate dust loading leads to greater total fluxes (more negative) compared to No-dust, while extreme dust amounts lead to a reduction in the total flux (less negative), which indicates less longwave radiation is escaping. The increase in total flux aloft for the moderate dust cases suggests a cooling effect; further, the radiative heating rates (Fig. 10b) also demonstrate a greater cooling effect. The combination of these influences leads to the slightly cooler temperature (Fig. 10c) above 600m in the moderate dust cases compared to No-dust. The warmer temperature in the column for the extreme dust, compared to No-Dust, is a result of the greater surface latent heat flux and diminished total radiative fluxes that offset the stronger radiative cooling from longwave flux divergence.

Deleted: ,

Deleted: no

Deleted: no

In the absence of solar radiation, the nighttime total radiative flux values are small relative to the daytime radiative quantities (e.g. Hansell et al., 2010; Marsham et al., 2016). As such, small changes in those factors impacting the radiation budget can more easily impact the ultimate balance in the heating or cooling near the ground and aloft at night. The dust impact on the radiative balance, and thus, the temperature profile at night, is only straightforward when comparing the No-Dust to the extreme dust simulations. More moderate dust events as in the Ginoux and Walker simulations do not produce consistent nighttime monotonic trends in the radiation fluxes with height. As discussed earlier, the low-level atmospheric temperature response to dust loading involves a complex interaction among the magnitudes of the total radiative fluxes, the ground surface heat fluxes, and the radiative heating/cooling rate (which is a function of the vertical attenuation rate or vertical flux divergence of the radiative fluxes). These controlling factors tend to have smaller magnitudes at night, thus making the net effect more sensitive to changes in dust loading. These results suggest that large dust loadings are necessary to generate consistent nighttime trends in radiation and temperature profiles, particularly above the surface. Otherwise, dust adds to the spread of uncertainty in these trends.

5 Summary and Conclusions

In this study, the direct radiative impact of dust and the resulting impact on the daytime and nighttime temperature profiles over extreme arid regions were examined in numerical simulations of a dust lofting event over the Arabian Peninsula (4-6 August 2016) that made use of three spatially varying specifications of surface dust erodible fraction. A simulation with no dust (labeled "No-Dust") was compared to simulations that used dust erodible fractions that were: (1) idealized with an erodible fraction of 1.0 in all land grid cells (labeled "Idealized"), (2) specified by the 1-degree resolution dataset from Ginoux et al. (2001) (labeled "Ginoux"), and (3) specified by the ~1km high-resolution data from Walker et al. (2009) (labeled "Walker"). Simulations were performed using both the RAMS and WRF-Chem models for comparison. The Idealized method of specifying erodible fraction has been shown to be useful in short term idealized type simulations (e.g. Seigel and van den Heever, 2012), but it likely represents the comparative upper bound of potential dust lofting and radiative responses in each respective model.

Both models revealed that Idealized dust lofting generates unrealistically high concentrations of dust mass and AOD, while the Ginoux and Walker simulations exhibited much more similarity. They also showed that use of the Ginoux and Walker dust erodible fraction databases reduces the amount of lofted dust compared to the Idealized method and brings the dust mass and AOD to within values closer to observations. RAMS simulations using the Ginoux and Walker databases generated AODs that were similar to MODIS and AERONET observations, while WRF tended to underestimate the AODs. The use of the high resolution erodible fraction database in the Walker simulations tended to produce more focused dust plumes with peak AODs that were higher than the those in the Ginoux simulations due to the identification of localized areas of high erodible potential. Meanwhile, the Ginoux simulations tended to produce more expansive plumes of moderately high AODs due to the more expansive area of moderate dust erodible fractions in the Ginoux database. However, the mean dust profiles from the analysis region in the RAMS simulations revealed only modestly higher dust concentrations in the Walker simulations compared to the Ginoux simulation. For the sake of brevity, the radiative impacts of dust from these simulations were presented solely from the RAMS simulations.

Due to the great variability in dust impacts on radiation between daytime and nighttime, our analyses treated these portions of the diurnal cycle separately and focused around the time of daytime maximal heating and nighttime maximal cooling. At either time, the resulting low-level temperature profile results from a combination of competing influences that include the magnitudes of shortwave and longwave radiative fluxes, radiative heating/cooling rates determined from the radiative flux divergence, and surface heat fluxes.

During the daytime, enhanced dust concentrations associated with surface dust lofting tend to reduce insolation, total radiative fluxes and surface heat fluxes, all of which induce a cooling effect. However, the stratification of dust in the lower atmosphere leads to enhanced radiative heating rates within these levels through changes in the radiative flux divergence which counteract the cooling effects of reduced total radiative flux magnitudes. The net result is a modest column warming effect for conditions of moderate dust concentrations in the Ginoux and Walker simulations. Thus, it appears that moderate dust loading may invoke strong responses in the profiles of upward and downward shortwave and longwave radiation while inducing only a small warming effect in the lower atmosphere. The extreme concentrations of dust in the Idealized simulations, while unrealistically high, demonstrate that the near-surface atmosphere will be substantially cooled, coupled with substantial warming aloft. This cooling occurs at the surface in the extreme dust case due to the large reduction in insolation overwhelming the increase in radiative heating rate. In summary, moderate dust amounts in the Ginoux and Walker simulations with constrained dust lofting tend to warm the near-surface and regions aloft while extreme dust amounts in the Idealized lofting simulation with unconstrained dust lofting tend to cool the near-surface layer and warm the regions aloft. The warming aloft increased with increasing dust loading from the Ginoux to Walker to Idealized simulations.

At night, the absence of solar radiation leads to much smaller total radiative and surface flux magnitudes which makes the resulting temperature profile more sensitive to small changes in the upward and downward longwave fluxes that comprise the total radiative flux. Dust effects on the radiative heating rates and radiative fluxes are more complex and not necessarily monotonic, which complicates assessing their impacts. The effect of increasing dust from the Ginoux to Walker to Idealized scenarios at night generates monotonically reduced total radiative fluxes (less negative) and increased latent heat fluxes near the surface, which overwhelms the non-monotonic increase in radiative cooling and leads to a slight warming near the surface. The near-surface warming is modest for the moderate dust cases but is more substantial for the extreme dust simulation. Above the lowest several hundred meters, however, the dust impact on temperature becomes non-monotonic due to corresponding non-monotonic trends in the radiative flux profiles. Drawing general conclusions of the impacts of dust on nocturnal temperature profiles is therefore difficult, since small fluctuations in the radiation streams and cooling rates can alter the signs of net heating/cooling. However, for moderate dust amounts in the Ginoux and Walker simulations, the above-surface temperature profiles promote slight cooling, while extreme dust loading promotes warming. In summary, increasing dust at night warms the atmosphere close to the surface but has variable effects above the surface layer depending on the dust amount; an extreme amount of dust tends to warm the surface and regions aloft.

Deleted: ed

The dust lofting simulations using databases of dust erodible fraction helped constrain the amount of dust lofting, thus, producing dust AODs that were comparable to the observed AODs in the associated dust plumes. In the mean radiative analysis of the Arabian dust plume over land, the presence of the simulated dust imposed substantial impacts on the individual shortwave and longwave radiative fluxes. However, shortwave and longwave fluxes tended to partially offset one another, and since the Arabian dust plume was weighted toward the surface, the in-plume radiative heating rates computed from the radiative flux divergence tended to compensate for the changes in the radiative fluxes. So, while the radiative impacts were substantial, the impact of the surface-based dust layer on the temperature profile in the lowest 2km was only ~1°C or less. We speculate that had the dust layer been weighted aloft, the surface daytime and nighttime temperature changes would have been larger in the absence of in-plume radiative heating which acted to offset the dust-induced changes in radiative fluxes at the surface.

Deleted:

The modification of surface heating and low-level temperature profiles by dust loading has important implications for the development and/or maintenance of mesoscale weather features that are generated in association with surface heating. Convection generated from heated thermals could be modified by daytime dust loading which could then in turn modify additional dust lofting associated with convective outflows. The thermodynamic impacts of dust loading could also impact sea breezes which are generated by differential daytime heating between ocean and adjacent land surfaces (Miller et al., 2003). Impacts on sea-breezes could then impact local dust concentrations and spatial distributions since onshore sea breeze winds have the potential to loft and transport dust and concentrate dust along sea breeze fronts (Verma et al., 2006; Igel et al., 2018). The size-dependent dust emission schemes can be further improved by using the constraints from both shortwave and longwave satellite measurements (Xu et al., 2017). The potential radiative impacts of dust on mesoscale features associated with the littoral zone will be examined in greater detail in future work.

Author Contributions

The dust database of Walker et al. (2009) and case overview was provided by Annette Walker. The Walker dust database was translated for the RAMS model by Jeremy Solbrig. AOD products associated with RAMS aerosols were generated by Python-based AOD software courtesy of Samuel Atwood, Qijing Bian, and Sonia Kreidenweis. MODIS Aqua and Terra aerosol AOD retrievals were processed and provided by Yi Wang and Jun Wang. MODIS Aqua true color imagery and case study guidance was provided by Steven Miller. WRF model analysis was provided by Jennie Bukowski. RAMS model analysis and data investigation was provided by Stephen Saleeby and Susan van den Heever. The majority of the manuscript was written by Stephen Saleeby, with all authors providing manuscript input and edits.

Deleted: ... [3]

Acknowledgements

This work was supported by the Office of Naval Research under Grant # N00014-16-1-2040 with project titled, "*Advancing Littoral Zone Aerosol Prediction via Holistic Studies in Regime-Dependent Flows"*. The simulation data are available upon request from the corresponding author, Stephen M. Saleeby. RAMS Initialization and nudging data provided by: National Centers for Environmental Prediction, National Weather Service, NOAA, U.S. Department of Commerce. 2000, updated

daily. *NCEP FNL Operational Model Global Tropospheric Analyses, continuing from July 1999.* Research Data Archive at the National Center for Atmospheric Research, Computational and Informational Systems Laboratory. https://doi.org/10.5065/D6M043C6.

References

Alfaro, S. C. and Gomes, L.: Modeling mineral aerosol production by wind erosion: Emission intensities and aerosol size distributions in source areas. J. Geophys. Res., 106, 18075-18084, doi:10.1029/2000JD900399, 2001.

Banks, J. R., Brindley, H. E., Hobby, M., and Marsham, J. H.: The daytime cycle in dust aerosol direct radiative effects observed in the central Sahara during the Fennec campaign in June 2011, J. Geophys. Res.-Atmos., 119, 13861–13876, doi:10.1002/2014JD022077, 2014.

Barnard, J., Fast, J., Paredes-Miranda, G., Arnott, W., and Laskin, A.: Technical Note: Evaluation of the WRF-Chem "Aerosol Chemical to Aerosol Optical Properties" Module using data from the MILAGRO campaign. Atmos. Chem. Phys., 10, 7325-7340, doi:10.5194/acp-10-7325-2010, 2010.

Bohren, C. F. and Huffman, D. R.: Absorption and scattering by a sphere, Absorpt. Scatt. Light Small Part., 82–129, doi:10.1002/9783527618156.ch4, 1983.

Carlson, T. N. and Caverly, R. S.: Radiative characteristics of Saharan dust at solar wavelengths. J. Geophys. Res., 81, 3141-3152, doi:10.1029/JC082i021p03141, 1977.

Carlson, T. N. and Benjamin, S. G.: Radiative heating rates for Saharan dust. J. Atmos. Sci., 37, 193–213, doi:10.1175/1520-0469(1980)037<0193:RHRFSD>2.0.CO;2, 1980.

Chou, M. D., and Suarez, M. J.: A solar radiation parameterization for atmospheric studies. NASA Tech. Memo. 104606, 15, 40pp, 1999.

Christopher, S. A., Wang, J., Ji, Q., and Tsay, S.-C.: Estimation of diurnal shortwave dust aerosol radiative forcing during PRIDE, J. Geophys. Res., 108, 8596, doi:10.1029/2002JD002787, 2003.

Cotton, W. R., Pielke, R. A., Sr., Walko, R. L., Liston, G. E., Tremback, C. J., Jiang, H., McAnelly, R. L., Harrington, J. Y., Nicholls, M. E., Carrió, G. G., and McFadden, J. P.: RAMS 2001: Current status and future directions. Meteorol. Atmos. Phys., 82, 5–29, doi:10.1007/s00703-001-0584-9, 2003.

Crosman, E. T. and Horel, J. D.: Sea and lake breezes: A review of numerical studies. Boundary-Layer Meteorol., 137, 1–29, doi:10.1007/s10546-010-9517-9, 2010.

Davies, H. C.: Limitations of some common lateral boundary schemes used in regional NWP models. Mon. Weather Rev., 111, 1002–1012, doi:10.1175/1520-0493(1983)111<1002:LOSCLB>2.0.CO;2, 1983.

Di Biagio, C., Formenti, P., Balkanski, Y., Caponi, L., Cazaunau, M., Pangui, E., Journet, E., Nowak, S., Andreae, M.O., Kandler, K., Saeed, T., Piketh, S., Seibert, D., Williams, E., and Doussin, J.-F.: Complex refractive indices and single

Formatted: Font:(Default) Times New Roman, 10 pt

Formatted: Left, Indent: Left: 0 mm, Hanging: 8.4 mm

Formatted: Font:(Default) Times New Roman, 10 pt

Formatted: Font:(Default) Times New Roman, 10 pt

Formatted: Font color: Black

scatter albedo of global dust aerosols in the shortwave spectrum and relationship to iron content and size. Atmos. Chem. Phys. Discuss., doi:10.5194/acp-2019-145.

Dubovik, O., Sinyuk, A., Lapyonok, T., Holben, B. N., Mishchenko, M., Yang, P., Eck, T. F., Volten, H., Muñoz, O., Veihelmann, B., van der Zande, W. J., Leon, J.-F., Sorokin, M., and Slutsker, I.: Application of spheroid models to account for aerosol particle nonsphericity in remote sensing of desert dust, J. Geophys. Res., 111, D11208, doi:10.1029/2005JD006619, 2006.

Eager, R. E., Raman, S., Wootten, A., Westphal, D., Reid, J., and Mandoos, A.: A climatological study of the sea and land breezes in the Arabian Gulf region. J. Geophys. Res., 113, D15106, doi:10.1029/2007JD009710, 2008.

Fast, J. D., Gustafson, W. I. Jr., Easter, R. C., Zaveri, R. A., Barnard, J. C., Chapman, E.G., and Grell, G. A.: Evolution of ozone, particulates, and aerosol direct forcing in an urban area using a new fully coupled meteorology, chemistry, and aerosol model. J. Geophys. Res., 111, D21305, doi:10.1029/2005JD006721, 2006.

Fecan, F., Marticorena, B., and Bergametti, G.: Parameterization of the increase of the Aeolian erosion threshold wind friction velocity due to soil moisture for arid and semi-arid areas. Ann. Geophys., 17, 149–157, doi:10.1007/s00585-999-0149-7, 1999.

Ge, C., Wang, J., and Reid, J. S.: Mesoscale modeling of smoke transport over the Southeast Asian Maritime Continent: couple of smoke direct radiative feedbacks below and above the low-level clouds, Atmos. Chem. Phys., 14, 159-174, doi:10.5194/acp-14-159-2014, 2014.

Giles, D. M., Holben, B. N., Eck, T. F., Sinyuk A., Smirnov, A., Slusker I., Dickerson, R. R., Thompson, A. M., and Schafer, J. S.: An analysis of AERONET aerosol absorption properties and classifications representative of aerosol source regions, J. Geophys. Res., 117, D17203, doi:10.1029/2012JD018127, 2012.

Ginoux, P., Chin, M., Tegen, I., Prospero, J.M., Holben, B., Dubovik, O., and Lin, S.-J.: Sources and distributions of dust aerosols simulated with the GOCART model. J. Geophys. Res., 106, D17, 20255-20273, doi:10.1029/2000JD000053, 2001.

Goudie, A. S. and Middleton, N. J.: Desert Dust in the Global System, Springer, Heidelberg, 2006.

Grell, G. A., Peckham, S. E., Schmitz, R., McKeen, S. A., Frost, G., Skamarock, W. C., and Eder, B.: Fully coupled 'online' chemistry in the WRF model. Atmos. Environ., 39, 6957-6976, doi:10.1016/j.atmosenv.2005.04.027, 2005.

Hansell, R. A., Tsay, S. C., Ji, Q., Hsu, N. C., Jeong, M. J., Wang, S. H., Reid, J. S., Liou, K. N., and Ou, S. C.: An assessment of the surface longwave direct radiative effect of airborne Saharan dust during the NAMMA field campaign. J. Atmos. Sci., 67, 1048-1065, doi:10.1175/2009JAS3257.1, 2010.

Harrington, J. Y.: The effects of radiative and microphysical processes on simulated warm and transition season Arctic stratus, Ph.D. dissertation, Colorado State University, Atmospheric Science Paper 637, 289 pp., 1997.

Haywood, J., Francis, P., Osborne, S., Glew, M., Loeb, N., Highwood, E., Tanre, D., Myhre, G., Formenti, P., and Hirst, E.: Radiative properties and direct radiative effect of Saharan dust measured by the C-130 aircraft during SHADE: 1.

Deleted:

Solar Spectrum. J. Geophys. Res., 108, D18, doi:10.1029/2002JD002687, 2003.

Haywood, J. M., Allan, R. P., Culverwell, I., Slingo, T., Mil- ton, S., Edwards, J., and Clerbaux, N.: Can desert dustex- plain the outgoing longwave radiation anomaly over the Sa- hara during July 2003?, J. Geophys. Res., 110, D05105, doi:10.1029/2004JD005232, 2005.

Holben, B. N., Eck, T. F., Slutsker, I., Tanre, D., Buis, J. P., Setzer, A.: AERONET — A federated instrument network and data archive for aerosol characterization. Remote Sensing of Environment, 66, 1–16, doi:10.1016/S0034-4257(98)00031-5, 1998.

Holben, B. N., Tanre, D., Smirnov, A., Eck, T. F., Slutsker, I., Abuhassa, N.: An emerging ground-based aerosol climatology: Aerosol optical depth from AERONET. J. Geophys. Res., 106, 12067–12097, doi:10.1029/2001JD900014, 2001.

Hsu, N. C., Herman, J. R., and Weaver, C. J.: Determination of radiative forcing of Saharan dust using combined TOMS and ERBE data. J. Geophys. Res., 105, 20649–20661, doi:10.1029/2000JD900150, 2000.

Hsu, N. C., Jeong, M. J., Bettenhausen, C., Sayer, A. M., Hansell, R., Seftor, C. S., Huang, J., Tsay, S. C.: Enhanced deep blue aerosol retrieval algorithm: The second generation. J. Geophys. Res., 118, 9296–9315, doi:10.1002/jgrd.50712, 2013.

Iacono, M. J., Delamere, J. S., Mlawer, E. J., Shephard, M. W., Clough, S. A., and Collins, W. D.: Radiative forcing by long–lived greenhouse gases: Calculations with the AER radiative transfer models. J. Geophys. Res., 113, D13103, doi:10.1029/2008JD009944, 2008.

Igel, A.L., van den Heever, S. C., and Johnson, J. S.: Meteorological and land surface properties impacting sea breeze extent and aerosol distribution in a dry environment. J. Geophys. Res., 123, 22-37, doi:/10.1002/2017JD027339, 2018.

Janjic, Z. I.: The Step–Mountain Eta Coordinate Model: Further developments of the convection, viscous sublayer, and turbulence closure schemes. Mon. Wea. Rev., 122, 927–945, doi:10.1175/1520-0493(1994)122<0927:TSMECM>2.0.CO;2, 1994.

Kain, J. S. and Fritsch, J. M.: Convective parameterization for mesoscale models: The Kain-Fritsch scheme, in The Representation of Cumulus Convection in Numerical Models, vol. 24, edited by K. Emanuel and D. Raymond, pp. 165–170, Meteorol. Monogr., Am. Meteorol. Soc., Boston, doi:10.1007/978-1-935704-13-3_16, 1993.

Kinne, S., Lohmann, U., Feichter, J., Schulz, M., Timmreck, C., Ghan, S., Easter, R., Chin, M., Ginoux, P., Takemura, T., Tegen, I., Koch, D., Herzog, M., Penner, J., Pitari, G., Holben, B., Eck, T., Smirnov, A., Dubovik, O., Slutsker, I., Tanre, D., Torres, O., Mishchenko, M., Geogdzhayev, I., Chu, D. A., and Kaufman, Y.: Monthly averages of aerosol properties: A global compari- son among models, satellite data, and AERONET ground data. J. Geophys. Res.-Atmos., 108, 4634, doi:10.1029/2001JD001253, 2003.

Kokkalis, P., Al Jassar, H. K., Solomos, S., Raptis, P.-I., Al Hendi, H., Amiridis, V., Papayannis, A., Al Sarraf, H., and Al Dimashki, M.: Long-term ground-based measurements of aerosol optical depth over Kuwait City. Remote Sens., 10, 1807, doi:10.3390/rs10111807, 2018.

Formatted: Font:(Default) Times New Roman, 10 pt

Formatted: Left, Indent: Left: 0 mm, Hanging: 8.4 mm

Formatted: Font color: Black

Deleted:

Kosmopoulos, P. G., Kazadzis, S., Taylor, M., Athanasopoulou, E., Speyer, O., Raptis, P. I., Marinou, E., Proestakis, E., Solomos, S., Gerasopoulos, E., Amiridis, V., Bais, A., Kontoes, C.: Dust impact on surface solar irradiance assessed with model simulations, satellite observations and ground-based measurements. Atmos. Meas. Tech., 10, 2435–2453, doi:10.5194/amt-10-2435-2017, 2017.

Lau, K. M., and Kim, K. M.: Cooling of the Atlantic by Saharan dust. Geo. Res. Lett., 34, L23811, doi:10.1029/2007GL031538, 2007.

Levy, R. C., Mattoo, S., Munchak, L. A., Remer, L. A., Sayer, A. M.; Patadia, F., Hsu, N. C.: The collection 6 MODIS aerosol products over land and ocean. Atmos. Meas. Tech., 6, 2989–3034, doi:10.5194/amt-6-2989-2013, 2013.

Marsham, J. H., Parker, D. J., Todd, M. C., Banks, J. R., Brindley, L. G-C., Roberts, A. J., and Ryder, C. L.: The contrasting roles of water and dust in controlling daily variation in radiative heating of the summertime Saharan heat low. Atmos. Chem. Phys., 16, 3563-3575, doi:10.5194/acp-16-3563-2016, 2016.

Marticorena, B. and Bergametti, G.: Modeling the atmospheric dust cycle: 1. Design of a soil-derived dust emission scheme. J. Geophys. Res., 100, 16415-16430, doi:10.1029/95JD00690, 1995.

Mesinger, F. and Arakawa, A.: Numerical Methods Used in Atmospheric Models. GARP Publ. Ser. 17, vol. 1, 66 pp., WMO, Geneva, Switzerland, 1976.

Meyers, M. P., Walko, R. L., Harrington, J. Y., and Cotton, W. R.: New RAMS cloud microphysics parameterization. Part II. The two-moment scheme. Atmos. Res. 45, 3-39, doi:10.1016/S0169-8095(97)00018-5, 1997.

Middleton, N. J.: Dust storms in the Middle East. J. Arid Environ., 10, 83–96, 1986.

Miller, S., Keim, B., Talbot, R., and Mao, H.: Sea breeze: Structure, forecasting, and impacts. Rev. Geophys., 41(3), 1011, doi:10.1029/2003RG000124, 2003.

Miller, S. D., Kuciauskas, A. P. Liu, M., Ji, Q., Reid, J. S., Breed, D. W., Walker, A. L., and Mandoos, A. A,: Haboob dust storms of the southern Arabian Peninsula. J. Geophys. Res., 113, D01202, doi:10.1029/2007JD008550, 2008.

Morrison, H., Curry, J. A., and Khvorostyanov, V. I.: A new double moment microphysics parameterization for application in cloud and climate models. Part I: Description. J. Atmos. Sci., 62, 1665–1677, doi:10.1175/JAS3446.1, 2005.

Morrison, H., Thompson, G., and Tatarskii, V.: Impact of Cloud Microphysics on the Development of Trailing Stratiform Precipitation in a Simulated Squall Line: Comparison of One– and Two–Moment Schemes. Mon. Wea. Rev., 137, 991–1007. doi:10.1175/2008MWR2556.1, doi:10.1175/2008MWR2556.1, 2009.

Nakanishi, M. and Niino, H.: An improved Mellor–Yamada level 3 model: its numerical stability and application to a regional prediction of advecting fog. Bound. Layer Meteor. 119, 397–407. doi:10.1007/s10546-005-9030-8, 2006.

Nakanishi, M. and Niino, H.: Development of an improved turbulence closure model for the atmospheric boundary layer. J. Meteor. Soc. Japan, 87, 895–912. doi:10.2151/jmsj.87.895, 2009.

Niu, G.–Y. and Coauthors: The community Noah land surface model with multiparameterization options (Noah–MP): 1. Model description and evaluation with local–scale measurements. J. Geophys. Res., 116, D12109, doi:10.1029/2010JD015140, 2011.

Petters, M. D. and Kreidenweis, S. M.: A single parameter representation of hygroscopic growth and cloud condensation nucleus activity. Atmos Chem Phys, 7(8), 1961–1971, doi:10.5194/acp-7-1961-2007, 2007.

Pielke, R. A., Cotton, W. R., Walko, R. L., Tremback, C. J., Lyons, W. A., Grasso, L. D., Nicholls, M. E., Moran, M. D., Wesley, D. A., Lee, T. J., and Copeland, J. H.: A comprehensive meteorological modeling system – RAMS. Meteorol. Atmos. Phys., 49, 69–91, doi:10.1007/BF01025401, 1992.

Pierre, C., Bergametti, G., Marticorena, B., Mougin, E., Bouet, C., and Schmechtig, C.: Impact of vegetation and soil moisture seasonal dynamics on dust emissions over the Sahel. J. Geophys. Res., 117, D06114, doi:10.1029/2011JD016950, 2012.

Prakash, P. J., Stenchkov, G., Kalenderski, S., Osipov, S., Bangalath, H.: The impact of dust storms on the Arabian Peninsula and the Red Sea. Atmos. Chem. Phys., 15, 199–222, doi:10.5194/acp-15-199-2015, 2015.

Prospero, J. M., Ginoux, P., Torres, O., Nicholson, S. E., and Gill, T. E.: Environmental characterization of global sources of atmospheric soil dust identified with the Nimbus 7 Total Ozone Mapping Spectrometer (TOMS) absorbing aerosol product. Rev. Geophys., 40, 1002, doi:10.1029/2000RG000095, 2002.

Remer, L.A., Kaufman, Y.J., Tanré, D., Matto, S., Chu., D.A., Martins, J.V., Li, R.-R., Ichoku, C., Levy, R.C., Kleidman, R.G., Eck, T.F., Vermote, E., Holben, B.N.: The MODIS aerosol algorithm, products, and validation. J. Atmos. Sci. 62, 947–973, doi:10.1175/JAS3385.1, 2005

Saleeby, S. M. and Cotton, W. R.: A large-droplet mode and prognostic number concentration of cloud droplets in the Colorado State University Regional Atmospheric Modeling System (RAMS). Part I: Module descriptions and supercell test simulations. J. Appl. Meteorol., 43, 182–195, doi:10.1175/JAM2312.1, 2004.

Saleeby, S. M. and van den Heever, S. C.: Developments in the CSU-RAMS aerosol model: Emissions, nucleation, regeneration, deposition, and radiation. J. Appl. Meteorol. Climatol., 52, 2601–2622, doi:10.1175/JAMC-D-12-0312.1, 2013.

Saleeby, S. M., van den Heever, S. C., Marinescu, P. J., Kreidenweis, S. M., and DeMott, P. J.: Aerosol effects on the anvil characteristics of mesoscale convective systems, J. Geophys. Res. Atmos., 121, 10,880–10,901, doi:10.1002/ 2016JD025082.

Seigel, R. B. and van den Heever, S. C.: Dust lofting and ingestion by supercell storms. J. Atmos. Sci., 69 ,1453-1473, doi:10.1175/JAS-D-11-0222.1, 2012.

Shao, Y.: A model for mineral dust emission. J. Geophys. Res., 106, 20239-20254, doi:10.1029/2001JD900171, 2001.

Shell, K. M., and Somerville, R. C. J.: Direct radiative effect of mineral dust and volcanic aerosols in a simple aerosol climate model. J. Geophys. Res.-Atmos., 112, D03205, doi:10.1029/2006JD007197, 2006.

Skamarock, W. C., Klemp, J. B., Dudhia, J., Gill, D. O., Barker, D. M., Duda, M. G., Huang, X.-Y., Wang, W., and Powers, J. G.: A Description of the Advanced Research WRF Version 3. NCAR Tech. Note NCAR/TN-475+STR, 113 pp. doi:10.5065/D68S4MVH, 2008.

Deleted:

Formatted: Indent: Left: 0 mm, Hanging: 8.4 mm

Slingo, A., Ackerman, T. P., Allan, R. P., Kassianov, E. I., McFarlane, S. A., Robinson, G. J., Barnard, J. C., Miller, M. A., Harries, J. E., Russell, J. E., and Dewitte, S.: Observations of the impact of a major Saharan dust storm on the atmospheric radiation balance. Geophys. Res. Lett., 33, L24817, doi:10.1029/2006GL027869, 2006.

Smagorinsky, J.: General circulation experiments with the primitive equations. Mon. Weather Rev., 91, 99-164, doi: 10.1175/1520-0493(1963)091<0099:GCEWTP>2.3.CO;2, 1963.

Smirnov, A., Holben, B. N., Eck, T. F., Slutsker, I., Chatenet, B., and Pinker, R. T.: Diurnal variability of aerosol optical depth observed at AERONET (Aerosol Robotic Network) sites. Geophysical Research Letters, 29, doi:10.1029/2002GL016305, 2002.

Sokolik, I. N. and Toon, O. B.: Direct radiative forcing by anthropogenic airborne mineral aerosols. Nature, 381, 681–683, doi:10.1038/381681a0, 1996.

Stokowski, D.: The addition of the direct radiative effect of atmospheric aerosols into the Regional Atmospheric Modeling System (RAMS). M.S. thesis, Dept. of Atmospheric Science, Colorado State University, Atmospheric Science Paper 637, 89 pp., 2005.

Tanaka, T. Y. and Chiba, M.: A numerical study of the contributions of dust source regions to the global dust budget. Global Planet. Change, 52, 88–104, doi:10.1016/j.gloplacha.2006.02.002, 2006.

Tegen, I. and Fung, I.: Modeling of mineral dust in the atmosphere: Sources, transport and optical thickness. J. Geophys. Res., 99, 22897–22914, doi:10.1029/94JD01928, 1994.

Tegen, I. and Lacis, A. A.: Modeling of particle size distribution and its influence on the radiative properties of mineral dust aerosol. J. Geophys. Res., 101, 19237-19244, doi:10.1029/95JD03610, 1996.

Verma, S., Boucher, O., Venkataraman, C., Reddy, M. S., Muller, D., Chazette, P., and Crouzille, B.: Aerosol lofting from sea breeze during the Indian Ocean Experiment. J. Geophys. Res., 111, D07208, doi:10.1029/2005JD005953, 2006.

Walker, A. L., Liu, M., Miller, S. D., Richardson, K. A., and Westphal, D. L.: Development of a dust source database for mesoscale forecasting in southwest Asia. J. Geophys. Res., 114, D18207, doi:10.1029/2008JD011541, 2009.

Walko, R. L., Cotton, W. R., Meyers, M. P., and Harrington, J. Y.: New RAMS cloud microphysics parameterization: Part I. The single-moment scheme, Atmos. Res., 38, 29–62, doi:10.1016/0169-8095(94)00087-T, 1995.

Walko, R. L. and Coauthors: Coupled atmosphere–biophysics–hydrology models for environmental modeling, J. Appl. Meteorol., 39, 931–944, doi: 10.1175/1520-0450(2000)039<0931:CABHMF>2.0.CO;2, 2000.

Wang, H., Shi, G-Y, Zhu, J., Chen, B., Che H., Zhao, T.: Case study of longwave contribution to dust radiative effects over East Asia., Chin. Sci. Bull, 58, 3673-3681, doi:10.1007/s11434-013-5752-z.

Wang, J., Nair, U., and Christopher, S.A.: GOES-8 Aerosol optical thickness assimilation in a mesoscale model: Online integration of aerosol radiative effects, J. Geophys. Res., 109, D23203, doi:10.1029/2004JD004827, 2004.

Wang, J., Liu, X., Christopher, S. A., Reid, J. S., Reid, E. A., and Maring, H.: The effects of non-sphericity on geostationary satellite retrievals of dust aerosols, Geophys. Res. Lett., 30, 2293, doi:10.1029/2003GL018697, 2003.

Wang, Y., Wang, J., Levy, R. C., Xu, X., Reid, J. S.: MODIS retrieval of aerosol optical depth over turbid coastal water,

Formatted: Justified, Indent: Left: 0 mm, Hanging: 8.4 mm, Space After: 12 pt, No widow/orphan control, Don't adjust space between Latin and Asian text, Don't adjust space between Asian text and numbers, Tabs: 3.9 mm, Left + 12.7 mm, Left

Formatted: Font:

Remote Sens., 9, 595, doi:10.3390/rs9060595, 2017.

Westphal, D. L., Toon, O. B., and Carlson, T. N.: A case study of mobilization and transport of Saharan dust, J. Atmos. Sci., 45, 2145–2175, doi: 10.1175/1520-0469(1988)045<2145:ACSOMA>2.0.CO;2, 1988.

Xu, X., Wang, J., Wang, Y., Henze, D. K., Zhang, L., Grell, G. A., McKeen, S., Wielicki, B.: Sense size-dependent dust loading and emission from space using reflected solar and infrared spectral measurements: An observation system simulations experiment, J. Geophys. Res. Atmos., 122, 8233-8254, doi:10.1002/2017JD026677, 2017.

Yang, Z.–L. and Coauthors: The community Noah land surface model with multi-parameterization options (Noah–MP): 2. Evaluation over global river basins. J. Geophys. Res., 116, D12110, doi:10.1029/2010JD015140, 2011.

Table 1. Summary of RAMS model grid setup and simulation configuration.

Model aspect	Setting
Grid	Arakawa C grid (Mesinger and Arakawa, 1976) 2 grids: Grid 1 used for forcing Grid2 Grid 1: 432x422pts, Δx=Δy=15 km, Δt=30 s Grid 2: 950x950pts, Δx=Δy=2 km, Δt=6 s 50 Vertical Levels Δz = 75m lowest level stretched to 750m aloft Model top at ~22 km AGL
Initialization	GDAS-FNL re-analysis 1-degree data
Boundary conditions	Lateral boundary nudging from gridded reanalysis (Davies, 1983)
Land-surface model	LEAF-3 (Walko et al., 2000)
Cumulus parameterization	Kain-Fritsch parameterization (Kain and Fritsch, 1993) on Grid-1
Radiation scheme	Two-stream, hydrometeor-sensitive (Harrington, 1997) and aerosol-sensitive (Stokowski, 2005; Saleeby and van den Heever, 2013)
Turbulence scheme	Horizontal and vertical turbulent diffusion via Smagorinsky (1963)
Microphysics scheme	Two-moment bin-emulating bulk microphysics for eight hydrometeor species (Walko et al., 1995; Meyers et al., 1997; Saleeby and Cotton, 2004; Saleeby and van den Heever, 2013)

Table 2. Summary of WRF-Chem model grid setup and simulation configuration.

Model aspect	Setting
Grid	2 grids: one-way nesting grid setup Grid 1: 432x422pts, Δx=Δy=15 km, Δt=60 s Grid 2: 950x950pts, Δx=Δy=3 km, Δt=15 s 50 Vertical Levels (hybrid sigma-pressure) Model top at ~22 km AGL
Initialization	GDAS-FNL re-analysis 1-degree data
Boundary conditions	Lateral boundary nudging from gridded reanalysis (Davies, 1983)
Land-surface model	NOAH (Niu et al., 2011; Yang et al., 2011)
Cumulus parameterization	BMJ parameterization (Janjic, 1994) on Grid-1
Radiation scheme	RRTMG (Iacano et al., 2008) with aerosol optical properties (Barnard et al., 2010)
Boundary Layer scheme	MYNN Level 3 (Nakanishi and Niino, 2006,2009)
Microphysics scheme	Two-moment Morrison (Morrison et al., 2005,2009)
Aerosol module	GOCART model (Ginoux et al., 2001)

Table 3. Summary of Simulations.

Simulation Name	Simulation Description
No Dust	No dust lofting permitted.
Idealized	Dust erodible fraction of 100% for grid cells with appropriate soil type and minimal vegetation.
Ginoux	Use of Ginoux et al. (2001) 1°x1° erodible fraction dataset mapped to model domain.
Walker	Use of Walker et al. (2009) ~1km dust erodible fraction dataset mapped to model domain.

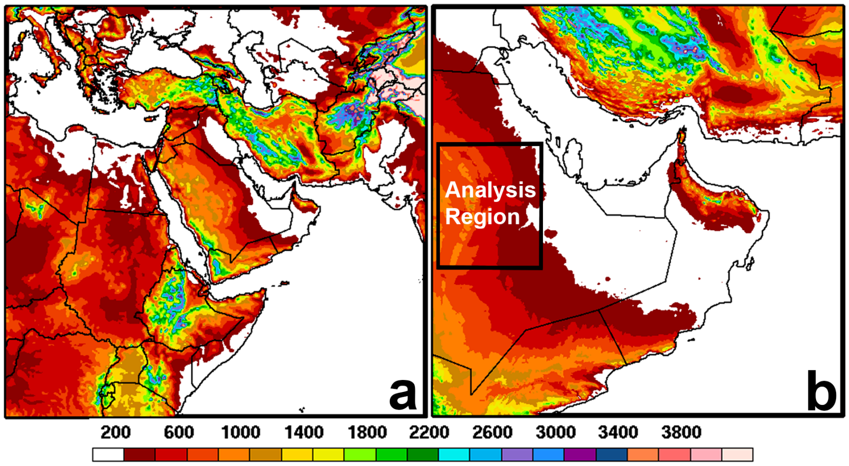

Figure 1. RAMS simulation domains with topography (shaded) for the domains with grid spacings of (a) 15km (Grid-1) and (b) 2km (Grid-2). The inset box denotes the dusty inland analysis region for the area-averaged time series and vertical profiles that follow.

5

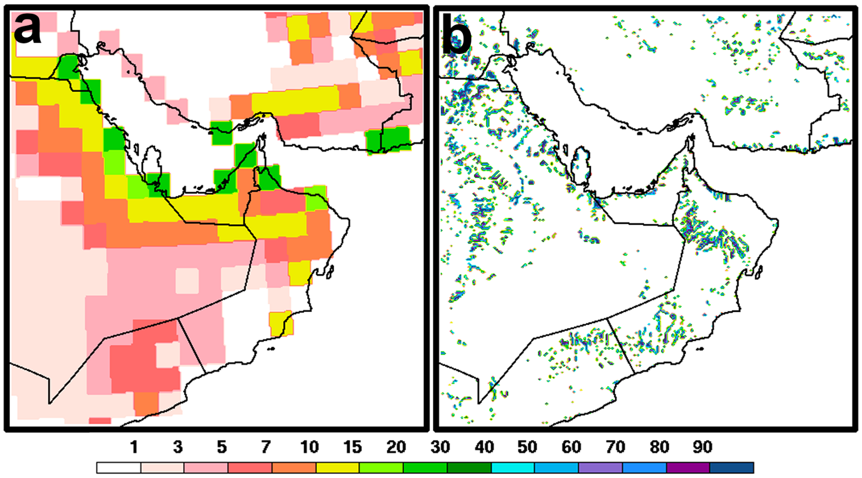

Figure 2. Erodible fraction potential for utilization in the dust lofting parameterization from (a) Ginoux et al. (2001) 1-degree dataset and (b) Walker et al. (2009) high resolution (1-km) database developed at the Naval Research Lab (NRL). Both datasets are shown mapped to the RAMS 2-km grid spacing domain. Values represent 0-100% erodible fraction.

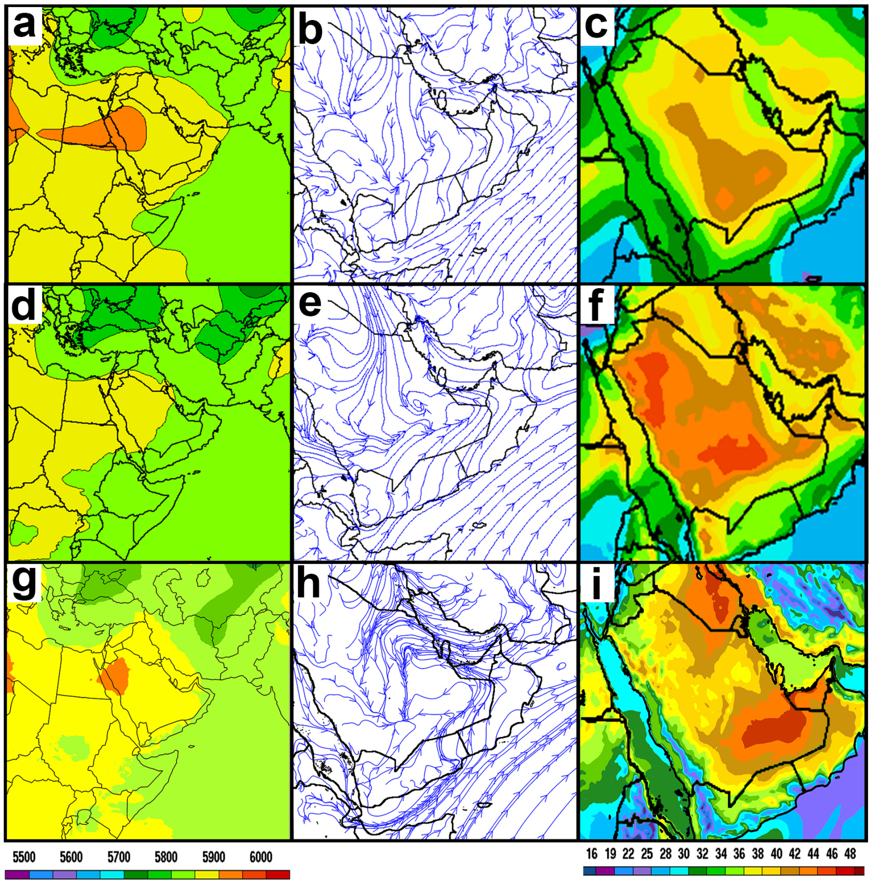

Figure 3. August 4, 2016 at 0000 UTC: (a,d,g) 500mb geopotential height (m), (b,e,h) 925mb streamlines, and (c,f,i) 1000mb temperature (C) from (a-c) GDAS-FNL, (d-f) RAMS Grid-1, and (g-i) WRF-chem Grid-1.

Deleted:

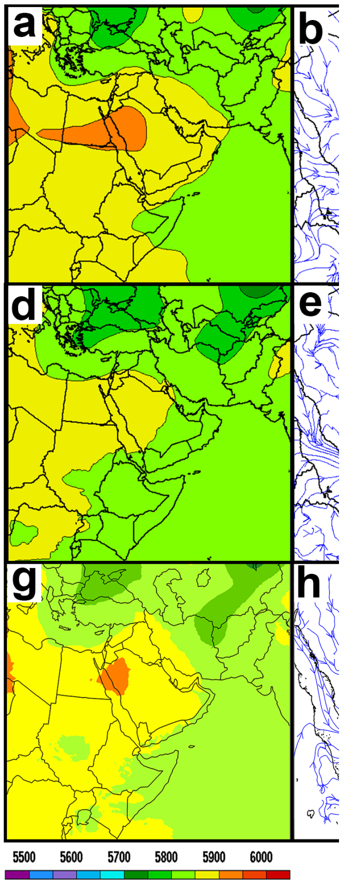

Formatted: Font:(Default) TimesNewRomanPS-BoldMT, 12 pt

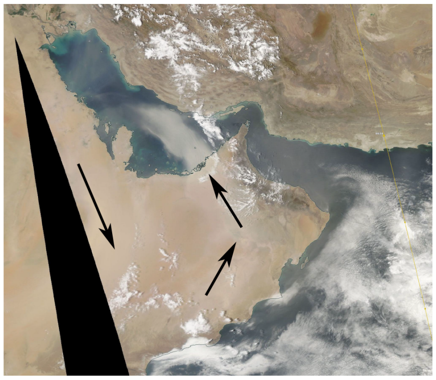

Figure 4. Snapshot of MODIS visible satellite image from 0930 UTC 4 August 2016. Arrows indicate the main direction of lofted dust advection and transport.

Deleted:

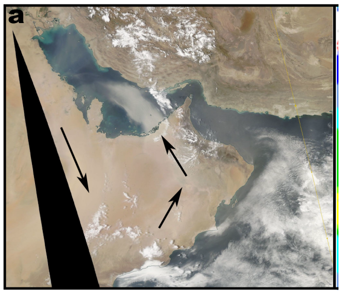

Formatted: Font:(Default) TimesNewRomanPS-BoldMT

Deleted: s

Deleted: (a)

Deleted: ,

Deleted: and (b) the NAAPS model surface dust mass concentration at 0600 UTC 4 Aug, 2016.

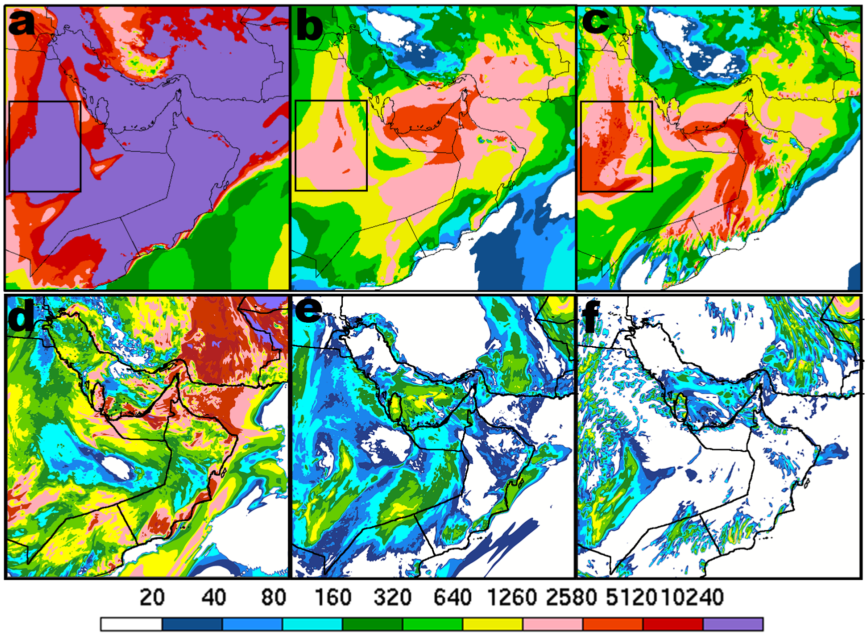

Figure 5. Simulated dust mass (ug/m3) at 0930 UTC 4 Aug, 2016 from the lowest model level (36m AGL) in RAMS and from the near-surface (945hPa) in WRF-chem using the (a,d) Idealized dust lofting, (b,e) Ginoux dust sources, and (c,f) Walker dust sources from the simulations from (a-c) RAMS and (d-f) WRF-chem. The black box over the central Arabian Peninsula denotes the analysis region shown in Figure 1.

Deleted:

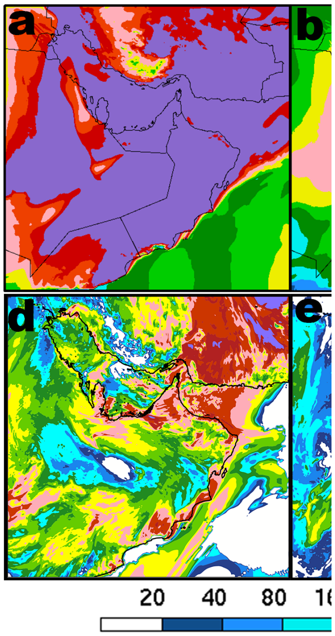

Formatted: Font:(Default) TimesNewRomanPS-BoldMT, 12 pt

Deleted: The color scale was set up to resemble that used in the NAAPS dust concentration image shown in Figure 4.

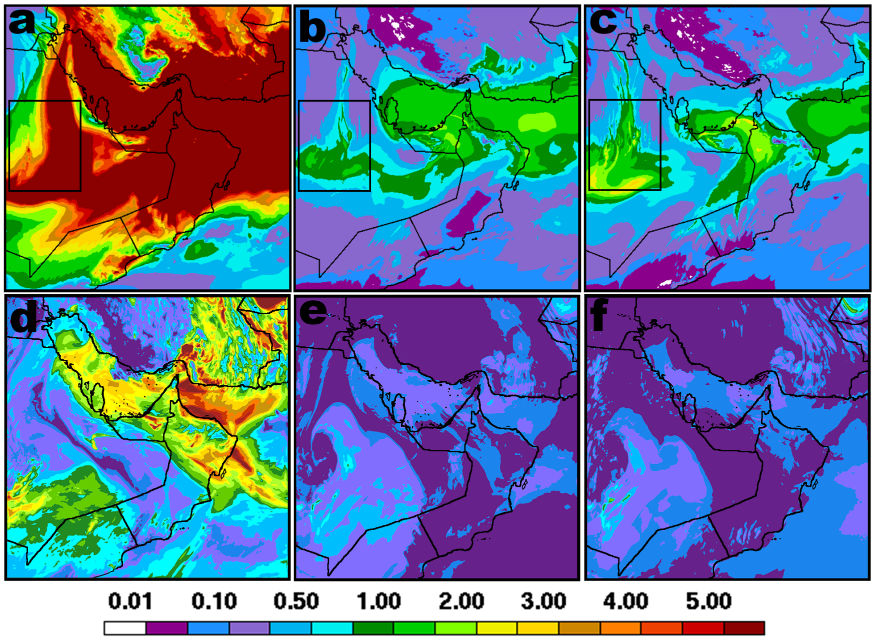

Figure 6. Simulated total AOD at 550nm from (a-c) RAMS and (d-f) WRF-chem simulations at 0930 UTC 4 Aug, 2016 using the (a,d) Idealized dust lofting, (b,e) Ginoux dust sources, and (c,f) Walker dust sources. The black box over the central Arabian Peninsula denotes the analysis region shown in Figure 1.

Deleted:

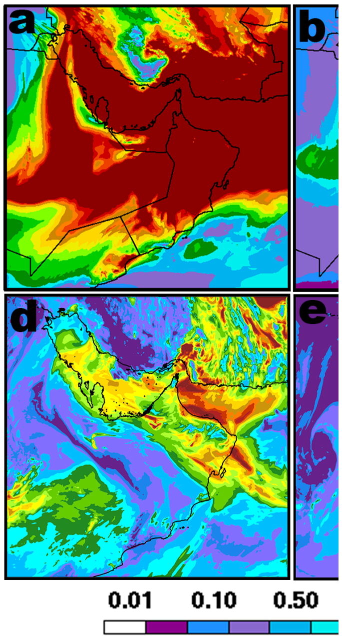

Formatted: Font:(Default) TimesNewRomanPS-BoldMT, 12 pt

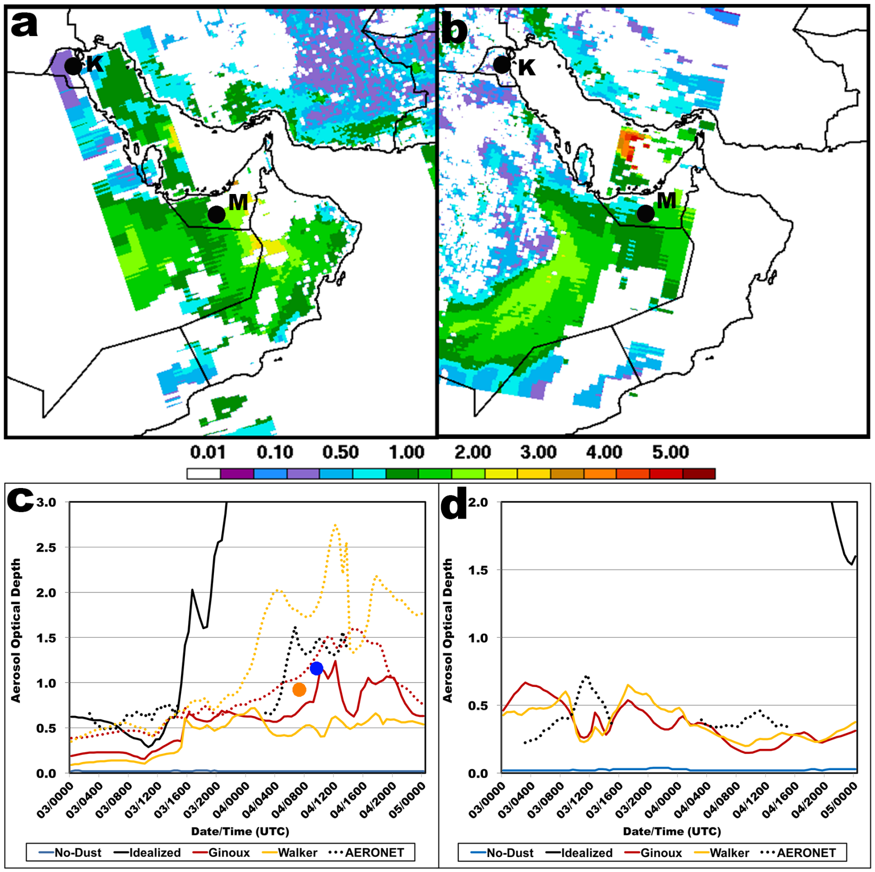

Figure 7. (a) MODIS Aqua AOD at 550nm at 0915 UTC 4 Aug, 2016, (b) MODIS Terra AOD at 550nm at 0745 UTC 4 August 2016, (c,d) time series of AERONET AOD at 500nm and modeled time series of AOD at 550nm at the locations of (c) Mezaira, UAE (23.11N, 53.76E, level 1.5 data) and (d) Kuwait University, Kuwait (29.33N, 47.97E, level 1.0 data). The black dots in panels a and b indicate the locations of AERONET stations at Kuwait University (K) and Mezaira (M). Colored, dotted lines in panel c correspond to the time series for an in-plume location 2-degrees east of the Mezaira site as discussed in the text. The large blue (red) dot in panel c indicates the MODIS Aqua (Terra) AOD that has been spatially interpolated to the Mezaira location from the retrievals in panels a and b.

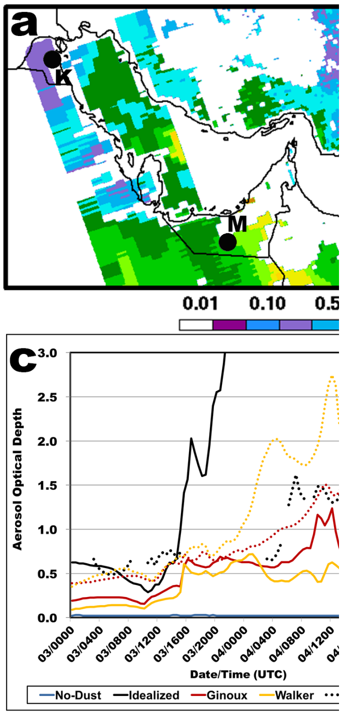

Deleted:

Formatted: Font:(Default) TimesNewRomanPS-BoldMT, 12 pt

Deleted: 1

Deleted: ,

Deleted: the

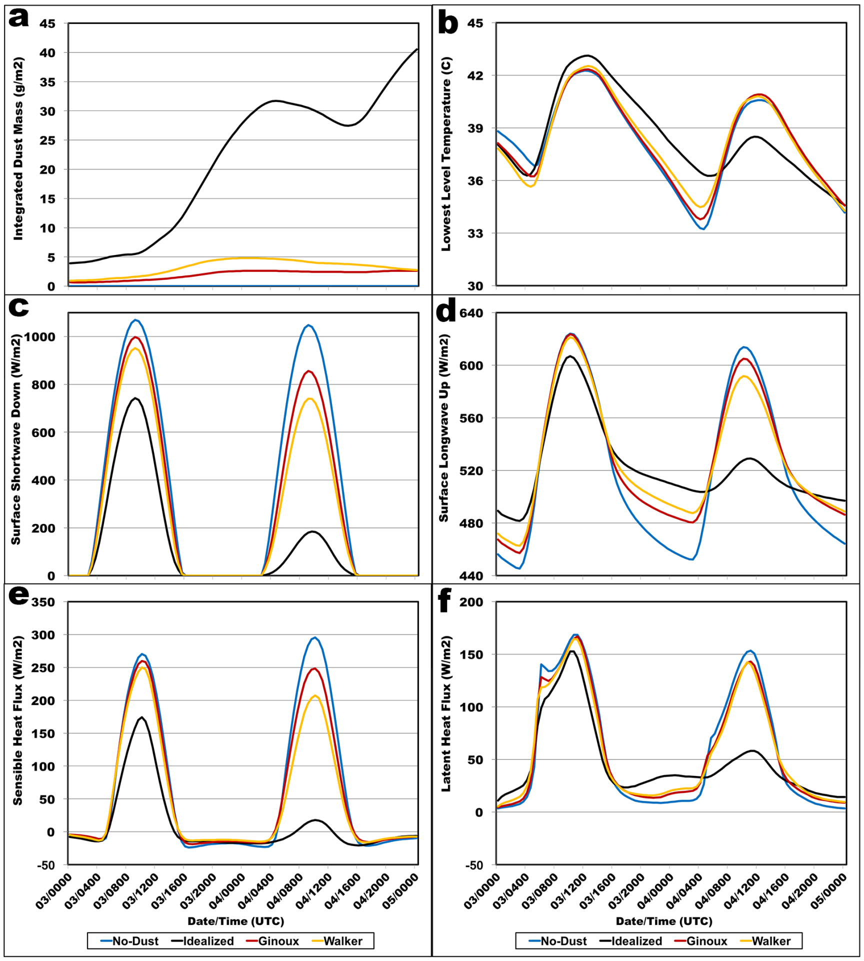

Figure 8. Time series of (a) vertically integrated dust mass (g m^{-2}), (b) lowest model level temperature (C), (c) surface downward shortwave radiation (W m^{-2}), (d) surface upward longwave radiation (W m^{-2}), (e) surface sensible heat flux (W m^{-2}), and (f) surface latent heat flux (W m^{-2}).

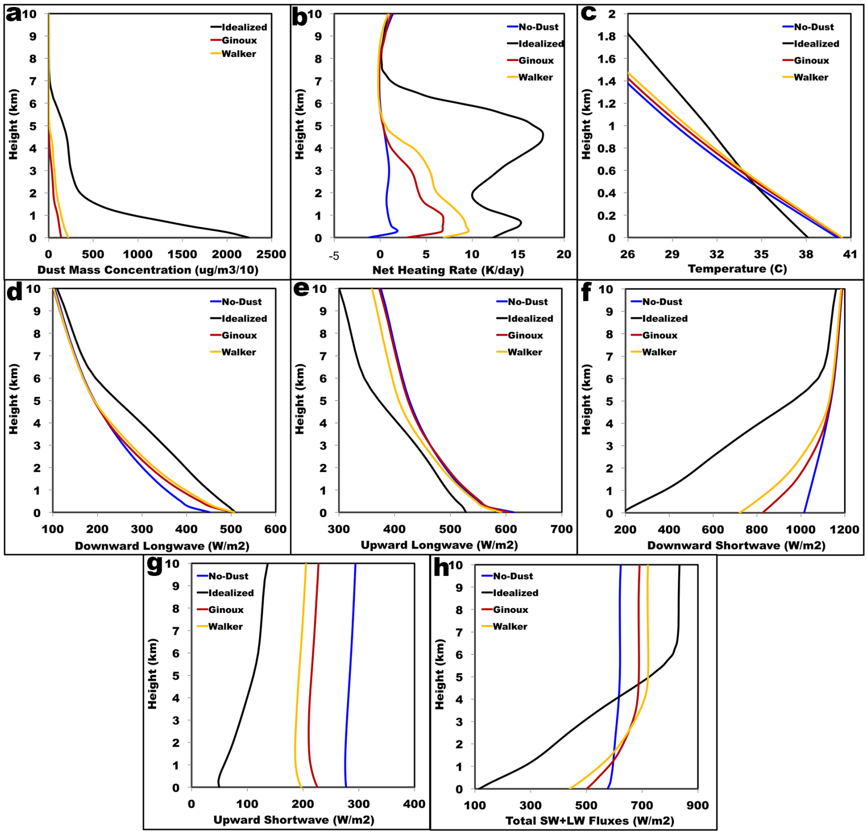

Figure 9. Daytime 1000 UTC (~1400 LST) 4 August vertical profiles of analysis-area averaged: (a) dust mass concentration (µg m^{-3} 10^{-1}), (b) net radiative heating rate (K day^{-1}), (c) temperature (C), (d) downward longwave (W m^{-2}), (e) upward longwave (W m^{-2}), (f) downward shortwave (W m^{-2}), (g) upward shortwave (W m^{-2}), and (h) total radiative fluxes (W m^{-2}) computed as the sum of shortwave and longwave, downward minus upward fluxes. Note that panel (c) is on a different vertical scale so as to zoom in on lower-level temperature.

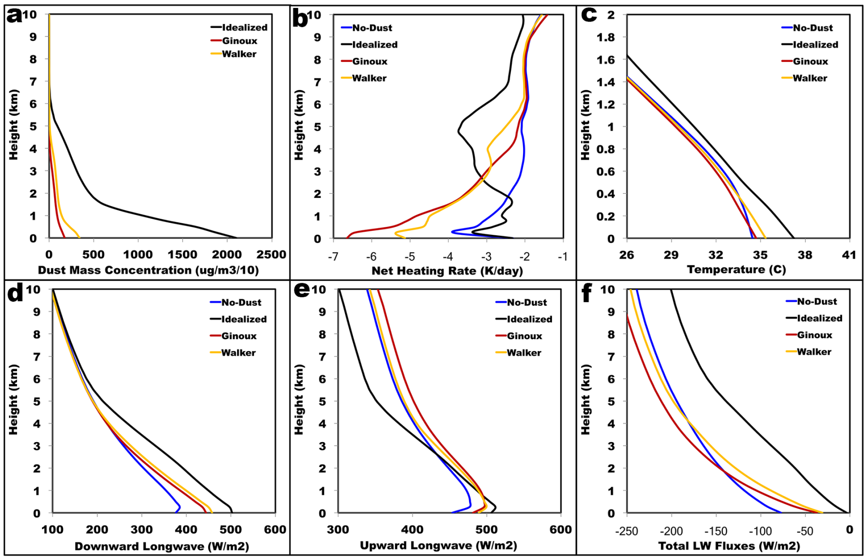

Figure 10. Nighttime 0200 UTC (~0600 LST) 4 August vertical profiles of analysis-area-averaged: (a) dust mass concentration (µg m^{-3} 10^{-1}), (b) net radiative heating rate (K day^{-1}), (c) temperature (C), (d) downward longwave (W m^{-2}), (e) upward longwave (W m^{-2}), and (f) total radiative fluxes (W m^{-2}) computed as the sum of shortwave and longwave, downward minus upward fluxes. Note that panel (c) is on a different vertical scale so as to zoom in on lower-level temperature.

Page 2: [1] Deleted	Saleeby,Stephen	5/7/19 1:00:00 PM

Page 8: [2] Deleted	Saleeby,Stephen	5/16/19 4:28:00 PM

Page 20: [3] Deleted	Saleeby,Stephen	5/23/19 2:10:00 PM